FACULDADE DE ENGENHARIA DA UNIVERSIDADE DO PORTO

Measuring Impedance in Congestive Heart Failure

Ricardo Reis Marques Silva

Mestrado Integrado em Engenharia Eletrotécnica e de Computadores

FEUP Supervisor: Jaime dos Santos Cardoso

Fraunhofer Portugal Supervisor: Filipe Sousa

July 27, 2016

Resumo

A hospitalização de doentes com insuficiência cardíaca tem cada vez maior peso nas despesas públicas, estima-se que no mundo inteiro existam cerca de 23 milhões de doentes que sofrem de insuficiência cardíaca, em Portugal serão aproximadamente 260,000. Os idosos são os mais afetados e com a esperança média de vida e os perfis de risco (diabetes e obesidade, por exemplo) a aumentar estima-se que estes numeros continuem a crescer.

A medição da impedância corporal está cada vez mais presente em ambiente clínico para avaliar a hemodinâmica. O risco de descompensação em doentes de insuficiência cardíaca pode ser avaliado com recurso à medição da impedância toráxica.

A progressão da doença está marcada por uma retenção gradual de fluído nos pulmões, muito antes dos sintomas de doença serem visíveis, é assim importance haver uma monitorização constante que permita detectar a acumulação de fluídos muito antes da hospitalização para que estes casos possam ser tratados.

No mercado não existem soluções de baixo custo e portáteis que permitam ao doente comum auto-diagnosticar-se de forma continua sem a necessidade de se deslocar a um hospital. Este trabalho propõe uma solução de custo reduzido, baixo consumo e pequenas dimensões (permitindo a portabilidade) que pode ser controlada através de um dispositivo móvel, por exemplo um smartphone.

Com esse intuito foi desenvolvido um sistema electrónico à volta dos Pandlets, que é uma plataforma desenvolvida pela Fraunhofer AICOS para medir o comportamento humano e o contexto ambiental. Este sistema é constítuido por um bloco responsável por gerar a corrente a ser injectada, outro bloco responsável pela aquisição do sinal e ainda um circuito de potência que permite que a alimentação do sistema seja feita através de uma simples bateria recarregável.

Ao criar uma comunicação Bluetooth Low Energy entre o dispositivo e um smartphone permite que um utilizador comum controle a medição de impedância através de uma App Android.

A solução desenvolvida apresenta um baixo consumo permitindo assim ser transportada no dia-a-dia pelo utilizador e trata-se de uma solução de baixo custo relativamente às outras presentes no mercado.

Os resultados apresentados nos testes realizados permitiram validar a viabilidade desta solução para a medição de impedância. No futuro serão implementadas as funções para a extracção dos parametros de Cole podem vir a ser implementados permitindo no futuro esta solução ser testada e implementada em ambiente clínico, para que os cardiologistas possam validar esta solução.

Abstract

The hospitalization of patients with Heart Failure represents an increasing burden for the health-care system, more than 23 million worldwide suffer from HF and in Portugal there are approximately 260,000. Living longer with multiple chronic diseases such as diabetes, kidney disease and heart failure is now the norm and not the exception and explains why increases in life expectancy among older adults are slowing.

Measuring body impedance is becoming increasingly available in the clinical setting as a tool for assessing hemodynamics, and can be used to measure the thoracic impedance in order to identify patients at risk for decompensation of heart failure.

The disease progression is marked by a gradual retention of fluid in the lungs, long before symptoms of disease worsening occur. In order to prevent this significant mortality, morbidity and healthcare expenditures it is necessary to monitor patients at risk, in a way to detect congestion episodes before worsening of symptoms that will lead to hospitalization.

There is not available in the market a portable and low-cost solutions that allows the commun user to auto-diagnose in a continuous way, not needing to go to the hospital . This work proposes a low-cost, low-power and small size solution (allowing the portability) that can be controlled by a mobile device, for example a smartphone.

With that in mind, an electronic system was developed built around Pandlets that is a platform developed by Fraunhofer AICOS to measure human behaviour and environmental context. This system is composed by a block responsible for generating a current to be injected, and another block to acquire the signal. A power circuit was also developed allowing the system to be supplied by a simple rechargeable battery.

The Smartphone uses Bluetooth Low Energy to comunicate with the device and to start the measurement procedure and estimate the thoracic impedance an Android App was created.

It can be observed that the proposed solution has a low power consumption so it can be carried by the user on a daily basis and when compared with the other solutions available on the market has a low cost of production.

The results of the tests performed help us to validate bioelectrical measurement method, some fields like the extraction of Cole Parameters can be implemented in the future, so this solution can be tested in a clinical setting, thus the cardiologists should validate the final solution.

Agradecimentos

Daqui a umas horas tenho que entregar este documento e chega a hora desta fatídica tarefa, que é agradecer às pessoas que de alguma forma contribuíram com algo positivo durante estes últimos anos na escola de Engenharia, e consequentemente para o desenvolvimento desta tese.

Já ando há algumas semanas a adiar este momento porque tenho sempre medo de cair naqueles clichés, mas vai ter que ser até porque seria injusto se não referisse algumas pessoas. Para terem ideia até estou a ouvir a "Golden Days" dos Whitney em loop, para ver se sai alguma coisa...

Vou fazer isto numa espécie de lista, porque bem, quem é que não gosta de listas?

- À Fraunhofer pelas excelentes condições e recursos que me disponibilizou durante este semestre;
- Ao meu orientador na Fraunhofer, Filipe Sousa, por toda a disponibilidade e boa disposição no dia-a-dia que sem dúvida ajudaram a chegar ao resultado que apresento neste documento;
- Ao professor Jaime Cardoso por todo o rigor científico com que contribuiu para este trabalho e por ter aceite orientar esta tese mesmo que numa primeira fase eu estivesse a 7000km de distância;
- Ao André Pereira, Carlos Resende, João Oliveira e Manuel Monteiro por toda a ajuda que deram no desenvolvimento desta tese, sem vocês definitivamente não teria os mesmos resultados;
- Aos meus amigos de Esmoriz por nunca me deixarem ter uma vida normal, quando estamos todos juntos parece um casamento cigano, pelo menos nunca ficamos Abandonados;
- Aos meus amigos da faculdade, tenha sido na associação, queimódromo, salas de estudo, biblioteca, laboratórios, salas de aula ou até mesmo nos inúmeros restaurantes por onde os Esteves passaram ficam memórias que levo comigo para a vida, como diz a canção;
- Às pessoas mais doentes que conheço e com quem tive a sorte (?) de partilhar uma casa/chat, fico apenas feliz por ainda não termos sido presos;
- À minha família por ser uma verdadeira família;
- Ao meu amigo André por em todos estes anos ter sido o irmão mais velho que nunca tive;
- À Mariana por ser o meu suporte e a pessoa mais importante na minha vida.

Se me tiver esquecido de alguém depois ainda dá para alterar na versão final.

Ricardo Silva

"I want to consistently play well and win titles.
I'm only at the beginning."

Cristiano Ronaldo

Contents

List of Figures

List of Tables

Abbreviations

ADC	Analog-to-Digital Converter
AICOS	Assistive Information and Communication Solutions
API	Application Programming Interfaces
AQD	Analog Quadrature Demodulation
ATT	Attribute Protocol
BIA	Bioelectrical Impedance Analysis
BLE	Bluetooth Low Energy
BoM	Bill of Materials
CCCD	Client Characteristic Configuration Descriptor
CFA	Current-Feedback Amplifier
CHF	Congestive Heart Failure
DAC	Digital-to-Analog Converter
DDS	Direct Digital Synthesis
DQD	Digital Quadrature Demodulation
DSP	Digital Signal Processing
DUT	Device Under Test
ECF	Extracellular Fluid
EIS	Electrical Impedance Spectroscopy
EIT	Electrical Impedance Tomography
EMU	Environmental Measurement Unit
FCC	Federal Communications Commission
GAP	Generic Access Profile
GATT	Generic Attribute Profile
GPD	Gain-Phase Detector
HCI	Host Controller Interface
HF	Heart Failure
I2C	Inter-Integrated Circuit
ICF	Intracellular Fluid
ICG	Impedance Cardiography
IEEE	Institute of Electrical and Electronics Engineers
IETF	Internet Engineering Task Force
IMU	Inertial Measurement Unit
INA	Instrumentation Amplifier
IoT	Internet of Things
IPG	Impedance Plethysmography
L2CAP	Logical Link Control and Application Protocol

LS	Left-Sided
MISO	Master In / Slave Out
MOSI	Master Out / Slave In
MRPDD	Magnitude-Ratio and Phase-Difference Detection
MSB	Most Significant Bit
NCO	Numerically Controlled Oscillator
OE	Output Enable
OTA	Over-the-Air
P2P	Point-to-Point
PAN	Personal-Area Network
Pandlets	Personal Area Dots: Letting Everything Sense
PCB	Printed Circuit Board
PSD	Phase Sensitive Detector
RF4CE	Radio Frequency for Consumer Electronics
RS	Right Sided
SCL	Serial-Clock Line
SD	SoftDevice
SDA	Serial-Data Line
SDK	Software Development Kit
SIG	Special Interest Group
SM	Security Manager
SMD	Surface Mount Devices
SPI	Serial Peripheral Interface
SVC	Supervisor Call
USA	United States of America
UUID	Universally Unique Identifier
VCCS	Voltage Controlled Current Source

Chapter 1

Introduction

1.1 Context

The healthcare system is overloaded with patients hospitalized due to Heart Failure (HF); in the United States of America (USA) more than 5.8 million suffer from HF and over 23 million worldwide. Every year more than 550,000 cases are diagnosed in the USA [17]. In Portugal there are approximately 260,000 individuals suffering from Heart Failure [18]. Elderly people are the most affected by HF problems, and considering the worsening risk factor profile for HF in the population (e.g. diabetes, hypertension), aging of the population (due to the longer life span), and the increasing HF prevalence, it is likely that these numbers will increase [19].

HF represents also a considerable burden to the healthcare system being responsible for costs of more than $39 billion annually in the USA. In developed countries, HF hospitalization represents 1-2% of all healthcare expenditures [17].

The American Heart Association defines Heart Failure as "a chronic, progressive condition in which the heart muscle is unable to pump enough blood through to meet the body's needs for blood and oxygen"; in a more simple way it means that the heart cannot keep the pace of the blood circulation.

Within the Heart Failure we can distinguish three different types:

- Left-Sided (LS) heart failure – when heart is pumping, it transports oxygen-rich blood from the lungs to the left atrium, then on to the left ventricle, which distributes it for the whole body. The pumping power of the heart comes mostly from the left ventricle so it is larger than the other chambers and essential for all the process. We can also distinguish the LS heart failure in two different types:
  - Systolic Failure – The left ventricle is not able to contract normally, so the heart cannot pump with enough force to push enough blood into circulation.
  - Diastolic Failure – The left ventricle loses the ability to relax normally and the heart cannot fill with blood during the period between each beat.

- Right Sided (RS) heart failure – the blood returns to the heart through the veins through the right atrium into the right ventricle. The blood is pumped into the lungs by the right ventricle to be provided with oxygen. The RS heart failure usually occurs due to LS heart failure. If the left ventricle fails, the pressure of the fluid increases which is transferred to the lungs, damaging the heart's right side. When this side loses the pump power, the blood goes back in the body's veins, causing swelling or congestion in the legs, ankles and swelling within the abdomen.

- Congestive Heart Failure (CHF) – if the blood flow out of the heart slows down, the blood coming back to the heart from the veins backs up, causing congestion in the body's tissues. Often swelling (edema) results. Sometimes fluid accumulates in the lungs and interferes with breathing. This is called pulmonary edema.

This thesis focuses on the CHF, monitoring the fluid status of the body. Current guidelines for assessing the fluid status of patients with heart failure include subjective physical findings, which often occur late in decompensation, and objective pulmonary artery catheter measurements, whose use is controversial in patients with heart failure [20].

1.2 Motivation

Measuring the impedance of the human body is becoming increasingly available in the clinical setting as a tool for assessing hemodynamics and volume status [21], and can be used to measure the thoracic impedance in order to identify patients at risk for decompensation of heart failure.

The study will be carried in association with Fraunhofer Portugal Research Center for Assistive Information and Communication Solutions (AICOS) and will be part of the international project SmartBEAT that focuses on developing useful and realistic services that reduce the need for hospital admissions and institutional care, and encourages early discharge.

The disease progression is marked by a gradual retention of fluid in the lungs, long before symptoms of disease worsening occur [22]. When patients are admitted at the hospitals with CHF they are usually suffering from symptoms such as dyspnea and edema and are treated with diuretic therapy.

In order to prevent this significant mortality, morbidity and healthcare expenditures it is necessary to monitor patients at risk, in a way that the fluid overload is detected long before the hospitalization.

1.3 Objectives

The aim of this study is to explore methods to detect fluid retention in the lungs by measuring the thoracic impedance, so it is possible to monitor Congestion Heart Failure patients, and physicians can early detect acute episodes.

To acquire the data it will be measured the thoracic impedance so it can be determined the accumulation of fluid in the lungs. Materials, such as blood or muscle, have a higher conductivity in comparison to bones or fat [23], and a lung filled with liquid has a higher conductivity than an air-filled one.

The purpose of the work is to develop a small and portable device to extract thoracic impedance of the patient. The solution should be low cost and friendly to use so it can be operated by a big range of users and also have a low power consumption for portable use.

The possibility that a patient can monitor his own body fluid by himself at home and be observed remotely by a doctor, would help to reduce drastically the number of hospitalizations and, consequently, improve the quality of live of people diagnosed with heart failure.

1.4 Contributions

The main contributions of this thesis are:

- Hardware and Firmware - Using the Magnitude-Ratio and Phase-Difference Detection (MR-PDD) method initially proposed by [2] and explained later in this document a structure will be constructed around the pandlets platform capable of measuring the thoracic impedance;
- Implementation of a bluetooth low energy communication - This will allow the use of a wireless connection capable of remote and real time monitoring by connecting the measuring device with a smartphone;
- Development of an Android application - With a user-friendly android app it will be possible to send and receive data from the measuring device allowing a continuous monitorring;
- Integration in the pandlets platform - By developing the measurement structure around pandlets, in the future this project could be integrated in a multi-parameter measuring application, since this platform allows to measure a wide number of variables.

1.5 Structure of the Document

Following this introduction a review of the literature regarding the bioelectrical impedance measurement will be made. Analysing both Bioelectrical Impedance Monitoring and Measurement Methods. Still in Chapter 2, follows a brief study of the solutions available in the market as also the other options for detecting HF events. The current Low-Power Technologies will also be previewed since one of the objectives of this work is to develop a device capable of communicate with a smartphone. In the last section of this Chapter a summary will be made.

After understanding how the Bioelectrical Impedance can be measured, in Chapter 3 the architecture used to develop the measurement device is presented, following in Chapter 4 the implementation of this architecture is explained.

The results of the work performed will be presented in Chapter 5, by testing the measurement device in a controlled environment and discussing the advantages of the features introduced by this thesis.

The conclusions and what can still be done to improve this study will be described in the last Chapter.

Chapter 2

State of the Art

In this chapter the state of the art regarding bioelectrical impedance measurement is presented. The different methods for bioelectrical impedance monitoring will be reviewed and advantages and disadvantages of these impedance methods will be discussed.

Since the goal is to develop a low-cost and low-power device capable of communicate with a mobile equipment, the current commercial solutions as well as different methods to measure impedance will be analysed.

2.1 Introduction to Bioelectrical Impedance

The human body is a biological system with a very complex structure composed by several living tissues [24]. Therefore the determination of the body composition and hemodynamics with noninvasive techniques represents a big challenge nowadays.

As referred before, materials, such as blood or muscle, have a higher conductivity in comparison to bones or fat and a lung filled with air has a lower conductivity than one filled with fluid. The biological cells, containing Intracellular Fluid (ICF), cell membranes with or without cell wall, are suspended in the Extracellular Fluids (ECF) and show a frequency behavior similar to an alternating electrical signal. If an alternate current is applied to the biological cells and tissues, a complex bioelectrical impedance, also known as bioimpedance, is produced which depends on tissue composition and the frequency of the applied signal [25].

The ECF and ICF are considered electrically resistive, whereas the cellular membrane, due to its lipid layer, has an isolating (capacitive) behavior, figure 2.1. According to that, the injected current will flow differently for low and high frequencies: low frequency current only flows around the cells through the ECF (R_e), whereas at high frequency current will also pass through the cell membranes and the ICF (C_m, R_i) [26].

The multifrequency studies provide a lot more information about the tissue properties which help in a better tissue characterization. Therefore the multifrequency impedance analysis is found very promising for noninvasive investigation of pathologies and physiological status.

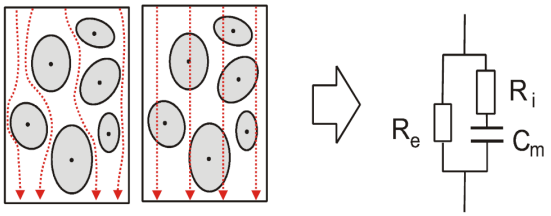

Figure 2.1: Low and high frequency current flow through body tissue. (In: [1])

2.2 Cole Equation

A very common practice within the multi-frequency bioelectrical impedance measurement is the fitting of the measured data to the Cole equation, using the Cole plot for data visualization and Cole parameters for data analysis.

Introduced by Kenneth S. Cole, in 1940 [27], the Cole equation is a mathematical equation that fits the experimentally obtained bioelectrical impedance measurements.

Using the Cole model, the frequency dependent impedance is described as follows:

$$Z(\omega) = \frac{R_e \cdot \left(R_i + \frac{1}{j\omega C_m}\right)}{R_e + R_i + \frac{1}{j\omega C_m}} = \left(\frac{R_e}{R_i + R_e}\right) \cdot \left(R_i + \frac{R_e}{1 + j\omega C_m (R_i + R_e)}\right) \tag{2.1}$$

with the following real and imaginary part:

$$Re\{Z\} = \frac{R_e + \omega^2 C_m^2 R_i R_e (R_i + R_e)}{1 + \omega^2 C_m^2 (R_i + R_e)^2} \tag{2.2a}$$

$$Im\{Z\} = \frac{\omega C_m R_e^2}{1 + \omega^2 C_m^2 (R_i + R_e)^2} \tag{2.2b}$$

The previously shown frequency dependent impedance would represent a semicircle in a complex frequency locus plot. Since real measurements show a depressed semicircle, a heuristic factor α as a tissue-specific dispersion parameter was introduced [28]. In that way, the electrical behaviour of biological tissue can be described completely by the Cole equation [29]:

$$Z(\omega) = R_\infty + \frac{R_0 - R_\infty}{1 + \left(j\frac{\omega}{\omega_c}\right)^\alpha} \tag{2.3}$$

where R_0 and R_∞ are the resistances at very low and high frequencies, respectively, ω_c is the characteristic angular frequency of the system and α is a dimensionless exponent .

2.3 Cole Parameter Extraction

The biolectrical impedance monitoring of a biological structure is normally obtained by measuring the real/resistive (R) and imaginary/reactive (X) impedance components, or the module (Z) and

phase angle (θ) [30].

As it can be observed in section 2.2, the Cole parameters (R_0, R_∞, α and τ) are the base of the multi-frequency bioelectrical impedance measurement and fitting the complex measurements data onto the Cole equation and then extracting the Cole parameters has become a common practice in multi-frequency bioelectrical impedance measurement applications [3].

When extracting the Cole parameters, it is usual to fit a semi-circular arc in the complex plane called the Cole plot, in which the resistive part R (on the horizontal axis) is plotted against the conjugate part of the reactance X (on the vertical axis). The fitted semi-circle travels through the original measured data according to certain rules from the right side to the left side along the locus as the frequency increases [27]. Cole plot is only an impedance plot, frequency information is not provided. R_0 and R_∞ are the intersections of the arc and the horizontal axis, α is a measure of the position of the center of the circle below the horizontal axis, τ corresponds to the inverse of the angular frequency ω of the impedance with highest reactance [31].

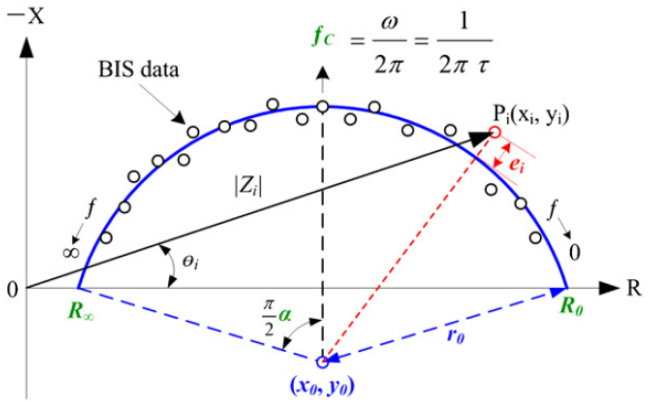

Figure 2.2: Cole Plot example (In: [2])

In order to estimate these parameters and having a curve and its mathematical function that approximates correctly the data points, a curve fitting technique needs to be applied. Regression analysis, to be more specific the non-linear least squares method is the most common approach to estimate the best coefficients of a defined non-linear model that fits the measured point to the curve described by the model [3]. The method tries to minimize the summed squared of the error between the data series and the fitted model as indicated:

$$min \sum_{i=1}^{N} e_i^2 = \sum_{i=1}^{N} (y_i - \overline{y_i})^2 \tag{2.4}$$

where e_i is the error of the *i-th* data point, and N is the total number of data points included in the fit.

By this relationship $j^\alpha = cos\left(\alpha \frac{\pi}{2}\right)$, it is possible to decompose the complex Z from the Cole equation into the real part, the resistance R and imaginary part, the reactance X, in the following

formulas:

$$R(\omega) = R_\infty + \frac{(R_0 - R_\infty)\left(1 + (\omega\tau)^\alpha cos\left(\alpha\frac{\pi}{2}\right)\right)}{1 + 2(\omega\tau)^\alpha cos\left(\alpha\frac{\pi}{2}\right) + (\omega\tau)^{2\alpha}} \tag{2.5a}$$

$$X(\omega) = -j\frac{(R_0 - R_\infty)1 + (\omega\tau)^\alpha sin\left(\alpha\frac{\pi}{2}\right)}{1 + 2(\omega\tau)^\alpha cos\left(\alpha\frac{\pi}{2}\right) + (\omega\tau)^{2\alpha}} \tag{2.5b}$$

Using the natural frequency as independent variable, for curve fitting we can estimate the Cole parameters R_0 R_∞, τ and α as the model coefficients.

The initial values are necessary and can be estimated from $R(\omega)$ and $X(\omega)$ planes of original data following the next method [3]:

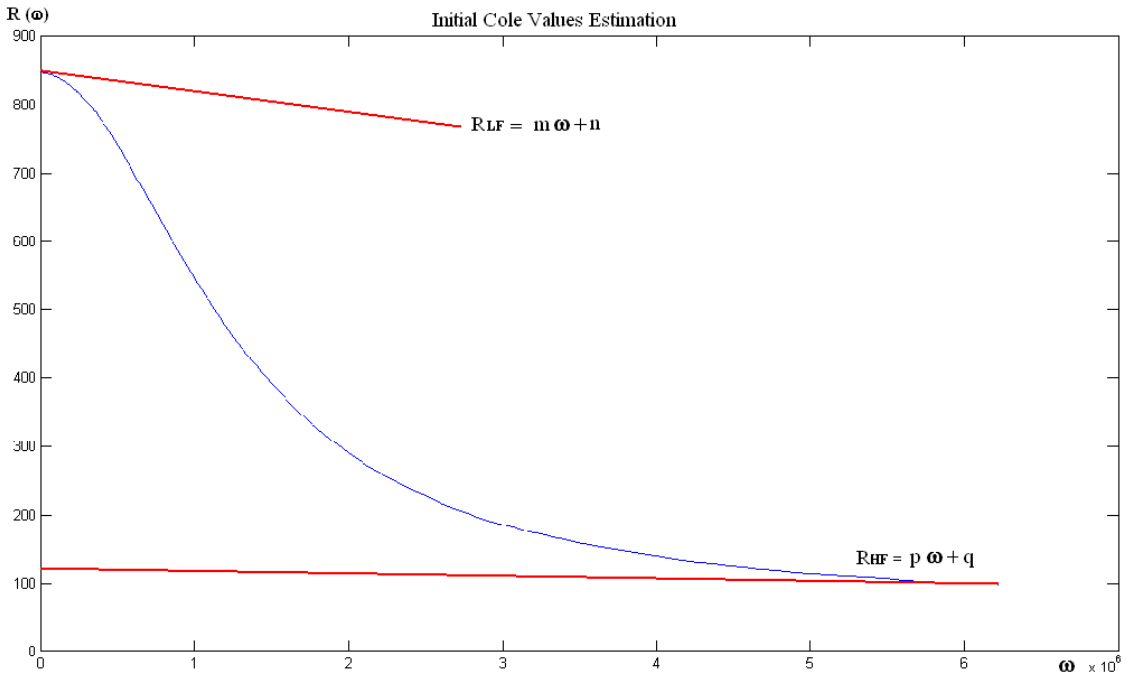

Figure 2.3: Regression lines for initial value estimation. (In: [3])

If the regression line R_{LF} is calculated as the line that fits the low frequency points of R, α can be estimated according to its slope:

$$\phi = -arctg(m) \tag{2.6a}$$

$$\alpha = \left(\frac{\pi}{2} - \phi\right) \cdot \frac{2}{\pi} \tag{2.6b}$$

R_0 can be estimated as the point where the line R_{LF} crosses the R axis, n, and R_∞ can be estimated as the point where the regression line at high frequencies R_{HF} crosses the R axis, q.

τ can be estimated from $X(\omega)$, taking into account that the maximum reactance is found at the characteristic frequency ω_C, and $\tau = 1/\omega_C$.

Since ECF and ICF contains ions, they are conducting and the measurements of their volume is based on their resistance or their impedance as celll membranes may act as capacitors at low and intermediate frequencies, this assumption allow us to calculate ECF and ICF as function of the Cole parameters [32].

2.4 Bioelectrical Impedance Monitoring Methods

Electrical impedance can be obtained by measuring the voltage developed across a particular part of an object when injecting a certain constant current signal to the object. Mathematically, the impedance (Z) is calculated dividing the voltage signal measured (V) by the current signal injected (I). Z is considered as a complex quantity, and it will have a phase angle (θ) depending on the tissue properties.

Many techniques are being used to study the frequency response of the electrical impedance of biological tissues; the following section presents the most commonly used in the literature.

2.4.1 Bioelectrical Impedance Analysis

The bioelectrical impedance $Z\angle(\theta)$ is calculated by dividing the voltage measured $V\angle(\theta_1)$ by applied current $I\angle(\theta_2)$ as shown in:

$$Z\angle(\theta) = \frac{V\angle(\theta_1)}{I\angle(\theta_2)} \tag{2.7}$$

In Bioelectrical Impedance Analysis (BIA) the body composition of a biological object is analysed by measuring its bioelectrical impedance. As explained before a constant sinusoidal current is injected to the subject under test, the voltage developed is measured using a four-electrode method, then the bioelectrical impedance is calculated. A constant alternate current is injected through the outer electrodes called current electrodes and the inner electrodes measure the voltage, known as voltage electrodes [33], as depicted in figure 2.4.

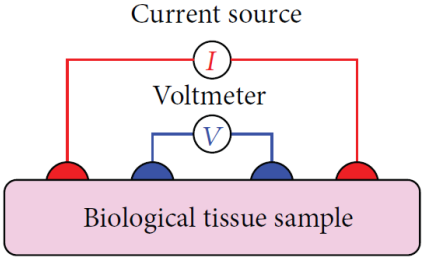

Figure 2.4: Impedance measurement using four-electrode technique. (In: [4])

A study on BIA was initiated in 1981 by Dr. William Mills, M.D., an Admiral in the US Navy who assessed the hydration status of soldiers in high altitude cold weather environments. In 1969 Hoffer et al. [34] published a paper indicating a procedure to predict the total body water by measuring the hand to foot whole body BIA (figure 2.5). Lukaski et al. [35] shortly after published the first paper on BIA and body composition.

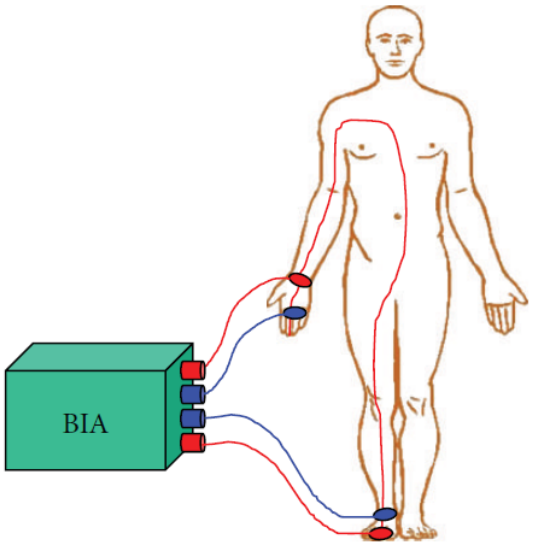

Figure 2.5: BIA current injection and voltage measurement schematic. (In: [4])

2.4.2 Electrical Impedance Spectroscopy

In this method the same principles explained before are applied, however in this technique the complex electrical impedance ($Z(f)$) and its phase angle ($\theta(f)$) of a subject under test are calculated at different frequency points by measuring the voltage ($V(f)$) developed for a constant current injection ($I(f)$).

Electrical Impedance Spectroscopy (EIS) is the most popular method for monitoring the bioelectrical impedance in several fields when compared with the other methods as it provides the impedance variations over a range of frequencies. Also EIS has been studied for the noninvasive characterization of biological as well as nonbiological materials in the frequency domain [4].

By studying the frequency response of the electrical impedance of any material the structural and compositional properties can be obtained as well as the frequency response of the material properties which can be potentially used for nondestructive material characterization.

Bioelectrical impedance only requires the placement of electrodes on the body in the classic tetrapolar arrangement on hand/wrist and foot/ankle for whole body measurement or in other positions for segmental measurements.

Using the impedance measurement over the entire spectrum of frequencies, the modeling procedure involves fitting the spectral data to the Cole equation using nonlinear curve fitting [27]. Thus the Cole model terms are generated, including R_e (resistance associated with the ECF); R_i

(resistance associated with the ICF); C_m (cell membrane capacitance); a heuristic factor (exponent α) that takes into account the distribution effects due to the tissue characteristics.

Cole model terms are then applied to equations derived from the Hanai mixture theory [36] which is based on the notion that the body is a conducting medium of water, electrolytes, and lean tissue, in addition to nonconducting material within it (eg, bone and fat). From this we can calculate ECF and ICF.

2.4.3 Impedance Plethysmography

Impedance Plethysmography (IPG) is an electrical impedance based noninvasive medical diagnostic procedure which measures small changes in the blood volume in terms of its bioelectrical impedance of a body part (figure 2.6), to study the tissue health condition of the patient.

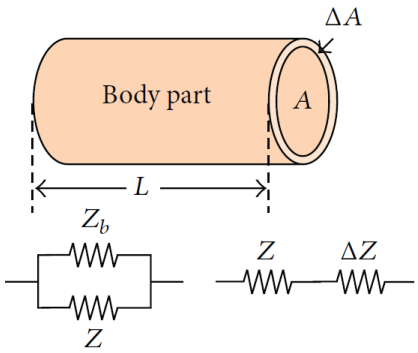

Figure 2.6: Volume change in body part due to blood pressure pulse and corresponding impedance variation due to the volume change. (In: [4])

A low amplitude, low frequency (50 kHz) alternate current is applied through the outer electrodes and the change in electrical impedance is measured across the inner electrodes, considering that is being used a four electrode placement technique.

IPG was proposed in early 1950's by Nyboer [37], by introducing the equations to evaluate volumetric change in the body parts in terms of impedance. Later a formula was proposed by Swanson and Webster [38], which is simpler both mathematically and computationally.

2.4.4 Impedance Cardiography

Impedance Cardiography (ICG) also referred to as transthoracic electrical bioimpedance, is a technology which calculates the changes in blood volume in transthoracic region over time, using the changes in transthoracic impedance [39] called thoracic electrical bioimpedance.

In the clinical setting, an alternating current (I), of constant magnitude, low amplitude (I_{RMS} = 1 - 4 mA) and frequency range from 30 to 100 kHz is injected through the thoracic volume, and the voltage change with each systole is measured. This change in voltage results in a change in thoracic impedance.

Electrodes are placed in an eight-electrode configuration (figure 2.7), where the current is introduced by electrodes placed on both sides of the neck and both sides of the lower thorax. The potential difference or voltage drop (E), is measured by another pair of electrodes below the current injecting electrodes on the neck, and another pair above the current injecting electrodes on the lower thorax.

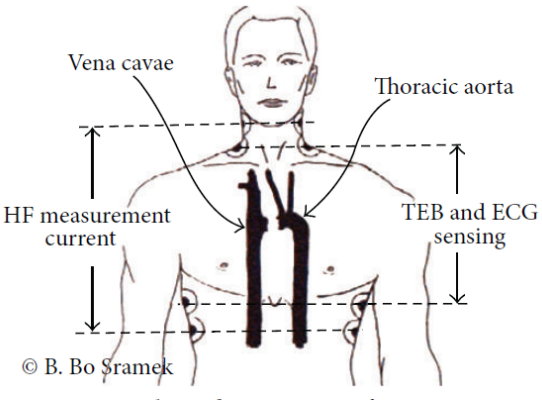

Figure 2.7: Impedance measurement with band electrode. (In: [4])

When this constant magnitude current is applied to the thorax, the voltage is proportional to the measured impedance. The overall thoracic impedance is called base impedance (Z_0). Z_0 is composed by the sum of weighted means of the various tissues impedance of the thorax including, fat, cardiac and skeletal muscle, lung, vascular tissue, bone, and the ratio of air to liquids in the thorax. The changes in impedance (ΔZ) correspond to both ventilation and pulsatile blood flow.

Analyzing Z_0 and ΔZ, the stroke volume, cardiac volume, and several hemodynamic parameters are calculated for noninvasive diagnosis of the heart and circulatory system.

2.4.5 Electrical Impedance Tomography

Electrical Impedance Tomography (EIT) [40], a computed tomography image reconstruction technique, is a nonlinear inverse problem in which the electrical conductivity or resistivity of a conduction domain (Ω) is reconstructed from the surface potentials developed by a constant current signal injected, figure 2.8, at the domain boundary ($\delta\Omega$).

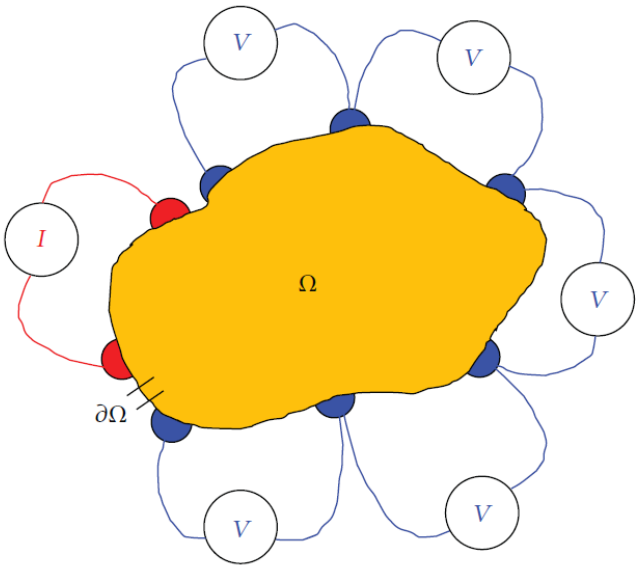

Figure 2.8: A closed domain of interest under EIT scanning with a constant current injection through driving electrodes and boundary potential measurement on sensing electrodes. (In: [4])

A low frequency, constant amplitude sinusoidal current is injected to the boundary ($\delta\Omega$) of the object domain (Ω) to be imaged within a volume conductor surrounded by an array of surface electrodes and the boundary potentials are measured using an electronic instrumentation [41].

The pair of electrodes called sensing electrodes collect the voltage data that is created by the current signal injected by the pair of electrodes called driving electrodes. Boundary data is then send to the PC that processes the data, constructing the spatial distribution of the domain under test using an image reconstruction algorithm.

EIT is a low cost, portable, fast, noninvasive, nonionizing and radiation free technique, and hence is found advantageous in several fields of applications compared to the other computed tomographic methods.

2.5 Bioelectrical Impedance Measurement Methods

The bioelectrical impedance is calculated as the complex division of the voltage measured over the tissue under test by the reference injected current. With the increasingly wide uses of the bioelectrical impedance techniques, a low cost, low power consumption, and capable of performing real-time measurement with adequate accuracy is highly desirable.

The two most commonly used methods for measuring the bioelectrical impedance of biological tissue are auto balancing bridge method and quadrature demodulation. More recently, a phase sensitive detector method that is gaining popularity with the advancement of the digital signal processing; another novel method uses the magnitude-ratio and phase-difference detection technique.

2.5.1 Auto Balancing Bridge Method

The current I_x flowing through the Device Under Test (DUT) (figure 2.9), flows also through the range resistor (R_r), by operation of the I-V converter. The potential at the Low point is maintained at zero volts (thus called a virtual ground), because the current through R_r balances with the one flowing through the DUT. The impedance of the DUT is calculated using the voltage measured at the High terminal (V_x) and across R_r (V_r) [5].

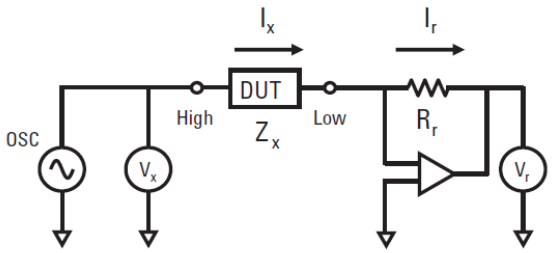

Figure 2.9: Auto-balancing bridge method circuit. (In: [5])

Another method known as the bridge method was traditionally the most popular method with the major advantage of high measurement resolution and accuracy. However, that method was time-consuming due to the need for bridge balance and not well suited in situations where tissue impedance changes in time due to ongoing physiological processes. That is the reason of the wide use of the auto balancing bridge method, instead of the traditional bridge method.

2.5.2 Analog Quadrature Demodulation

The classical Analog Quadrature Demodulation (AQD) method, as can be observed in figure 2.10, is based on phase coherent demodulation and needs two channels of well-matched in-phase (I) and quadrature (Q) references. In AQD, the need for carefully avoiding any mismatch between the I and Q channels, which will cause large phase errors, may cause some complexity in the circuit.

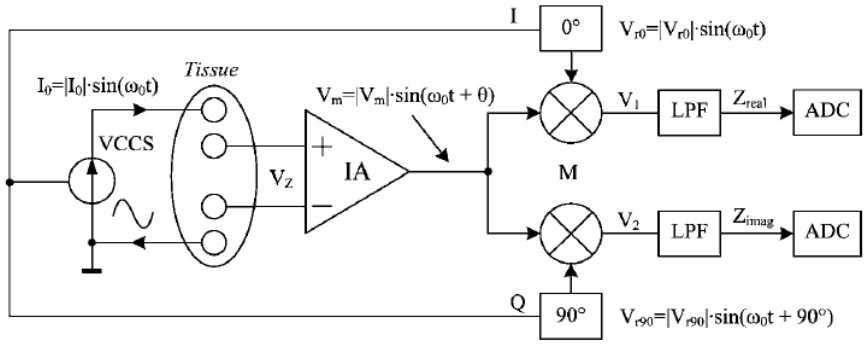

Figure 2.10: Block diagram of the conventional analog quadrature demodulation (AQD) method based on tetropolar structure. (In: [2])

With the development of Digital Signal Processing (DSP) techniques, direct sampling of the signals at the carrier frequency has become possible in recent years, which enables the evolution of AQD to Digital Quadrature Demodulation (DQD). DQD no longer requires the analog I and Q references. However, the need for high-speed Analog-to-Digital Converters (ADCs) and DSPs often leads to high costs and high power consumption because of the high sampling rate [2].

2.5.3 Phase Sensitive Detector

Nowadays Phase Sensitive Detector (PSD) is gaining popularity. PSD is a technique used in instrumentation and measurement systems, to extract the characteristics of a signal buried in noises [6]. One of the many applications is in the electrical impedance tomography systems, to recover the amplitude and phase information of the measured sinusoidal voltage signal, which could be buried in random noise due to the many disturbances, explained before.

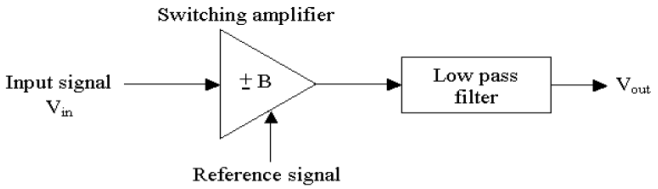

Figure 2.11: Block diagram of an analogue PSD circuit. (In: [6])

Traditionally, an analogue PSD circuit (figure 2.11), comprises a switching amplifier (whose gain is switched between $+B$ and $-B$) followed by a low-pass filter. Switching of the amplifier gain is controlled by a reference signal having the same frequency (f_c) as that of the input signal, v_{in}, whose amplitude A is the information to be extracted. The two signals, input and reference, have to be phase-locked, with phase difference Φ, which is not necessarily zero. The switching amplifier effectively acts as a synchronous full-wave rectifier for v_{in}, or as an analogue multiplier multiplying the input signal v_{in} with the square-wave reference signal. The low-pass filter, following the switching amplifier, extracts v_{out}, the dc component of the amplifier's output signal.

2.5.4 Magnitude-ratio and phase-difference detection

A novel method was introduced by Yuxiang Yang et al. [2] which provides a compact and cost-effective alternative for real-time impedance measurements. The principle of the Magnitude-Ratio and Phase-Difference Detection (MRPDD) can be observed in figure 2.12.

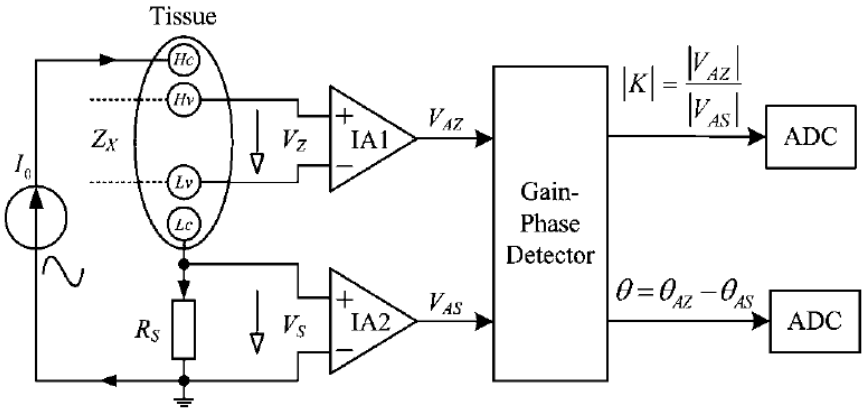

Figure 2.12: Impedance measurement principle based on the magnitude-ratio and phase-difference detection (MRPDD) method. (In: [2])

Z_X represents the impedance of the tissue under measurement, and R_S is a reference resistor connected in series with Z_X. A sinusoidal excitation current I_0 is injected through Z_X and R_S via two current electrodes H_c and L_c. A pair of voltage electrodes H_v and L_v detects the voltage drop across Z_X (V_Z) and then is amplified by instrumentation amplifier IA1, while the voltage drop across R_S (V_S) is amplified by a similar instrumentation amplifier IA2. The two output voltages of IA1 and IA2 can be expressed as (2.8), assuming that the input impedances of IA1 and IA2 are infinite and there will be no current flowing through the two voltage electrodes:

$$\begin{cases} V_{AZ} = A_1 \cdot V_Z = A_1 \cdot I_0 \cdot Z_X \\ V_{AS} = A_2 \cdot V_S = A_2 \cdot I_0 \cdot R_S \end{cases} \tag{2.8}$$

where A_1 and A_2 are the gains of IA1 and IA2, respectively.

The Gain-Phase Detector (GPD) is responsible to compare V_{AZ} and V_{AS}, outputing two DC voltages proportional to magnitude ratio $|K|$ and phase difference θ of the input voltages:

$$\begin{cases} |K| = \frac{|V_{AZ}|}{|V_{AS}|} \\ \theta = (\theta_{AZ} - \theta_{AS}) \end{cases} \tag{2.9}$$

By solving simultaneously both equations systems, we obtain the unknown impedance Z_X:

$$Z_X = R_S \cdot \frac{V_Z}{V_S} = R_S \cdot \frac{A_2}{A_1} \cdot \frac{V_{AZ}}{V_{AS}} = R_S \cdot \frac{A_2}{A_1} \cdot |K| \angle \theta \tag{2.10}$$

If the IA1 and IA2 were constructed identically and have an infinite input impedance, we assum the gain ratio as $A_2/A_1 = 1$. Then the previous equation is simplified and the originally measured impedance Z_m is obtained as:

$$Z_m = R_S \cdot |K| \angle \theta \tag{2.11}$$

where R_S is a standard resistor with known value.

2.6 Commercial Solutions

As seen before Bioelectrical Impedance Monitoring is gaining force in the clinical setting for monitoring body composition and hemodynamics noninvasively. This allows professional medical clinicians to monitor the status of the individual and prevent hospitalization.

Next is presented a review of some of those available bioelectrical impedance monitoring solutions on the market.

2.6.1 BioZ

Created by CardioDynamics [42] BioZ (figure 2.13), "is an innovative noninvasive ICG device that provides hemodynamic parameters based on the measurement of thoracic electrical bioimpedance. Specifically, the BioZ allows for assessment of a patient's hemodynamic status and ventricular function by determining twelve (12) hemodynamic parameters as well as four (4) indexed parameters".

Trends in the patient's status can be observed by the operator, measure blood pressure independently, view and store the collected data and waveforms, connect the data to a PC.

As presented before, it implements an ICG method that measures the change in impedance by injecting a high frequency (60 kHz minimum), low amplitude (4.0 mA RMS maximum) alternating electrical current through the thorax.

By detecting and measuring the change in thoracic impedance as a function of time, the BioZ is able to noninvasively calculate stroke volume, cardiac output and many other hemodynamic parameters.

Figure 2.13: BioZ Monitor. (In: [7])

2.6.2 Hydra 4200

Hydra 4200 (figure 2.14), produced by Xitron Technologies [43]. Xitron has been designing bioimpedance instrumentation and conducting impedance-body water research since 1985.

Xitron's uses a BIS technology that has been validated on a number of populations by a variety of leading body composition research institutions dating back to 1992 and was the first company to introduce a multifrequency device with a measurement range of 1 kHz to 1 MHz and full Cole modeling software.

It can be controlled by either a computer using the system utilities software or by the easy to use interface of the hydra 4200 that has an extensive number of data processing capabilities, thus, the Cole model can be computed internally without use of a computer.

Figure 2.14: Xitron Hydra 4200. (In: [8])

2.6.3 PF05 Lab1

PhysioFlow PF05 Lab1 [9] (figure 2.15), covers a range of medical devices designed to perform continuous non-invasive measurements of cardiac output. PhysioFlow developed a new technology based on ICG called SM-ICG.

ICG presented some limitations for it only works in normal or near normal patients and exclusively at rest or very moderate exercise. Obesity, pulmonary edema, emphysema, ventilation are some known limitations to ICG. It is very sensitive to electrodes placement and therefore not very reproducible from one operator to another.

SM-ICG uses a first level optimized input filter finely adapted to the high frequency current transmitted, so that the impedance signal measured is mostly free from noise coming from other electronic or physiologic devices.

SM-ICG also uses a second level highly sophisticated filter, called HD-Z (for High Definition Impedance) to eliminate all artifacts from the chest impedance signals that are not correlated with the heart cycle and the generation of cardiac flow. It has been developed to cancel severe artifacts in the most demanding situations like a running race or in a very noisy critical care environment.

Figure 2.15: PF05 Lab1 Bioelectrical Impedance Monitor. (In: [9])

2.6.4 Quantum IV

The Quantum IV (figure 2.16), is a BIA [44] produced by RJL Systems that permits to assess body composition. It is an instrument with good accuracy, reliability and ease of use.

The Quantum IV precisely measures resistance and reactance at 50 kHz; by positioning two electrodes in the right hand and other two in the right foot it is possible to measure the human biological resistance and reactance when the patient is in supine position.

Following the principles presented before regarding BIA, it is possible to determine the total body composition. With this device it is also possible through a software to automatically obtain the body composition connecting Quantum IV to a computer.

Figure 2.16: Quantum IV Monitor. (In: [10])

2.6.5 ZOE

The ZOE Fluid Status Monitor [11] (figure 2.17), "is a transportable thoracic bioimpedance monitor that provides measurement of fluid status".

Base impedance (Z_0) decreases when fluid increases and rises when less fluid exists in the chest. Normal thoracic Z_0 range is between 19-30 ohms, however every person has their own baseline. It is advised to note fluid status changes and share them with professional medical clinicians when Z_0 readings vary from typical daily values.

The advantage of this device is that it can be used by adults at home to autonomously monitor bioelectrical impedance changes. However ZOE is an assessment tool, it is not intended to be a medical diagnostic device. The physician or designated healthcare provider is responsible for interpreting what assessment, intervention, or action is required as a result of changing Z_0 values.

Figure 2.17: ZOE Fluid Status Monitor. (In: [11])

2.7 Other Options

2.7.1 Monitoring Daily Weight

Daily weight monitoring is strongly recommended by the American College of Cardiology/American Heart Association clinical practice guidelines and recommending it to patients is considered a measure of quality in HF care. Several recent investigations have reported relatively low sensitivity and specificity of changes in daily weight to predict worsening HF events [45].

A study conducted by Sarwat I. Chaudhry et al. [46] concluded that increases in body weight are associated with hospitalization for heart failure and begin at least 1 week before admission. Daily information about patients body weight identifies a high-risk period during which interventions to avert decompensated heart failure that requires hospitalization may be beneficial.

2.7.2 UWB Sensor

LifeWave Biomedical [47] created a solution for noninvasive body monitoring, the UWB Sensor is similar in concept to ultrasound but uses radio frequency instead of sound energy.

The LifeWave UWB sensor emits very low energy, which propagate into the human body. As the energy enters the body, small amounts of the incident energy are reflected back to a sensing device. The reflections are primarily the result of the differences in dielectric properties of the underlying tissues and organs. The reflected energy is then received and processed using signal processing algorithms to extract information on the type, location, size, and relative movement of the illuminated tissues and organs.

The LifeWave technology is safe for full-time usage and skin contact and meets all FDA human safety and Federal Communications Commission (FCC) regulations governing human RF exposure.

2.8 Low-Power Wireless Technologies

Wireless is a major feature for every electronic product. It adds flexibility, convenience, and remote monitoring and control without the expensive and inconvenient wiring and cabling. Many innovative new use cases are now being made possible with the introduction of ultra-low-power wireless chipsets. The application under development will be characterized by small amounts of sensor information between the measuring device and the central mobile device.

As one of the objectives of the work is to implement a low power communication between the measuring device and a mobile device, a study of the low power wireless communications available is in order.

2.8.1 ANT

ANT "is a low-power proprietary (but open access) wireless technology which operates in the $2.4GHz$. It was established in 2004 by the sensor company Dynastream. Typically, the ANT transceiver device is treated as a black box and should not require much design effort to implement into a network" [48]. As a type of personal-area network (PAN), ANT's primary applications include sports, wellness, and home health.

ANT+ is an interoperability function that can be added to the base ANT protocol. This standardization allows for the networking of nearby ANT+ devices to facilitate the open collection and interpretation of sensor data [49].

The technology divides the $2.4GHz$ industrial, scientific, and medical (ISM) band into $1MHz$ channels. The radios have a basic data rate of $1Mbit/s$. A time division multiplexing (TDM) scheme accommodates multiple sensors.

ANT+ supports star, tree, mesh, and peer-to-peer topologies. The protocol and packet format is simple. And, it boasts ultra-low power consumption and long battery life [50].

2.8.2 ZigBee

ZigBee "is a low-power wireless specification based on the Institute of Electrical and Electronics Engineers (IEEE) Standard 802.15.4-2003" and was established by a group of 16 companies in 2002 [48].

It provides a complete protocol stack designed to implement multiple types of radio networks that include point-to-point, tree, star, and point-to-multipoint. Its main feature is the possibility to build large mesh networks for sensor monitoring. It can handle up to 65,000 nodes. ZigBee also provides profiles or software routines that implement specific applications for consumer home automation, building automation, and industrial control [50].

ZigBee is not a frequency hopping technology, therefore it requires careful planning during deployment in order to ensure that there are no interfering signals in the proximity.

2.8.3 RF4CE

Radio Frequency for Consumer Electronics (RF4CE) is based on ZigBee and was standardized in 2009 by four consumer electronics companies: Sony, Philips, Panasonic, and Samsung. RF4CE is supported by two silicon vendors: Texas Instruments and Freescale Semiconductor, Inc. RF4CE's intended use is as a device remote control system, for example for television set-top boxes. The intention is that it overcomes the common problems associated with infrared: interoperability, line-of-sight, and limited enhanced features [48].

Zigbee RF4CE protocol stack utilizes $2.4GHz$ transceiver compliant to 802.15.4 for remote control devices and their targets (audio and video devices). The second RF4CE application profile is introduced in 2012 compliant to zigbee standard [51].

2.8.4 6LoWPAN

6LoWPAN means IPv6 protocol over low-power wireless PANs. The concept was born from the idea that the Internet Protocol could and should be applied to even the smallest of devices [52].

Developed by the Internet Engineering Task Force (IETF), it provides a way to transmit IPv6 and IPv4 Internet Protocols over low-power wireless point-to-point (P2P) links and mesh networks. This standard (RFC4944) also permits the implementation of the Internet of Things on even the smallest and remote devices [50].

Its characteristics make the technology ideal for markets such as home automation with sensors and actuators, street light monitoring and control, residential lighting, smart metering and generic IoT applications with Internet connected devices. Today's deployments use both $2.4GHz$ and Sub- $1GHz$, building on the IEEE 802.15.4 advantages including support for large mesh network topology, robust communication and very-low power consumption [53].

2.8.5 Bluetooth Low Energy

Bluetooth Low Energy (BLE), that is marketed as "Bluetooth Smart", "is a lightweight subset of classic Bluetooth and was introduced as part of the Bluetooth 4.0 core specification. While there is some overlap with classic Bluetooth, BLE actually has a completely different lineage and was started by Nokia as an internal project called "Wibree" before being adopted by the Bluetooth Special Interest Group (SIG)" [54].

As a result of being a standard, BLE benefits from all the advantages of conformance and extensive interoperability testing. A device that operates Bluetooth v4.0 may not necessarily implement other versions of Bluetooth; in such cases it is known as a single-mode device. New Bluetooth chipsets from leading Bluetooth silicon manufacturers will support Bluetooth and the BLE functionality [48].

Bluetooth Smart technology operates in the same spectrum range (the $2.400GHz - 2.4835GHz$ ISM band) as Classic Bluetooth technology, but uses a different set of channels. Instead of the Classic Bluetooth 79 $1MHz$ channels, Bluetooth Smart has 40 $2MHz$ channels.

2.9 Summary

It is important to have in mind that the purpose of this work is to develop a low-power and low-cost device capable of communicating with a mobile equipment, it should also be friendly to use so it can be operated by a big range of social classes.

Electrical impedance based noninvasive tissue characterizing techniques like bioelectrical impedance analysis (BIA), electrical impedance spectroscopy (EIS), electrical impedance plethysmography (IPG), impedance cardiography (ICG), and electrical impedance tomography (EIT) are being used to study the frequency response of the electrical impedance of biological tissues. But EIS is found more popular in several fields of application compared to BIA, IPG and ICG as it provides the impedance variations over frequencies.

Regarding the methods for measurement of the impedance the most important aspect is the low-power characteristic in order to develop a small size and portable device. Most of the methods presented in the literature are either time consuming or require the use of a DSP that results in the increase of the power consumption. The novel method using the MRPDD technique provides a feasible advantage over the traditional bioelectrical impedance measurement systems, based on quadrature demodulation methods, by simplifying the electronics.

Table 2.1: Commercial Solutions Resume

	Monitoring Method	Price
BioZ	ICG	5,800$
Hydra 4200	BIS	Not Available
FF05 Lab1	SM-ICG*	2,999$
Quantum IV	BIA	3,090$
ZOE	ICG	2,860$

*Method based on ICG

The bioelectrical devices currently on the market analyzed in this work are either based on ICG technology or EIS or BIA, as seen in table 2.1. The disadvantages of these devices is that none of them has an user friendly interface and portable size, and all of them have an expensive price for home monitoring. This represents a scientific and commercial opportunity that will be explored by this work.

The purpose of this work is to develop a cheaper solution than the ones available on the market that could be integrated in the daily use of the patients with the use of a mobile device. This mobile device (e.g. smartphone) would be responsible for the human-machine interaction, resulting in reduction of the price and a solution capable of direct connection to the physicians would allow remote monitoring.

In regard to the wireless communication there are plenty of protocols available, but BLE is the easiest and cheapest one to implement. Nowadays the Bill of Materials(BoM) for a system-on-chip solution with microcontroller and radio integrated is under 2$ which is well below the total overall price point of similar wireless technologies (ZigBee, RF4CE, 6LoWPAN, etc.).

Chapter 3

Proposed Architecture

3.1 Overview

The system will be built around pandlets (Personal Area Dots: Letting Everything Sense) (figure 3.1). A Pandlet is a platform developed by Fraunhofer AICOS to measure human behaviour and environmental context.

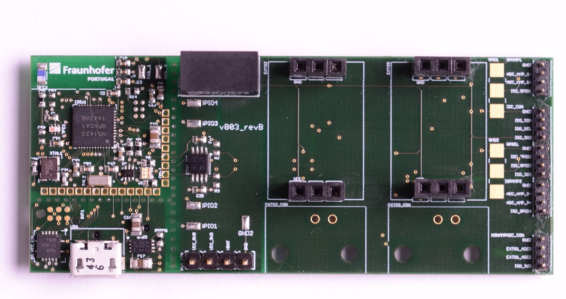

Figure 3.1: Pandlets Board.

The circuit that generates the excitation source includes a sine wave generator and a Voltage Controlled Current Source (VCCS) and will be responsible for generating the excitation current in a range of frequencies from $20kHz$ to $1MHz$.

Two equivalent Instrumentation Amplifiers (INA) will be used, one to amplify the signal measured by the pair of voltage electrodes and the other to amplify the voltage drop across the reference resistor, then the INAs two input buffers will be used to match the internal impedance of the GPD.

The voltage from the pair of electrodes and reference resistor is compared using the GPD and calculates magnitude ratio and phase difference.

With Pandlets, the analogic-digital conversion will be made and the data will be transferred to a smartphone using Bluetooth Low Energy (BLE), marketed as Bluetooth Smart.

Pandlets will also be responsible for tuning the signal generator and implementing the previously explained MRPDD method by acquiring the digital signal from the ADCs.

So the low-power feature can be achieved a power circuit is included in the design and a wireless communication will be implemented so a real time monitoring can be achieved between the device and a mobile phone.

A structual diagram of the device can be oberved in figure 3.2, the different blocks are separated by dashed lines and respectively labeled.

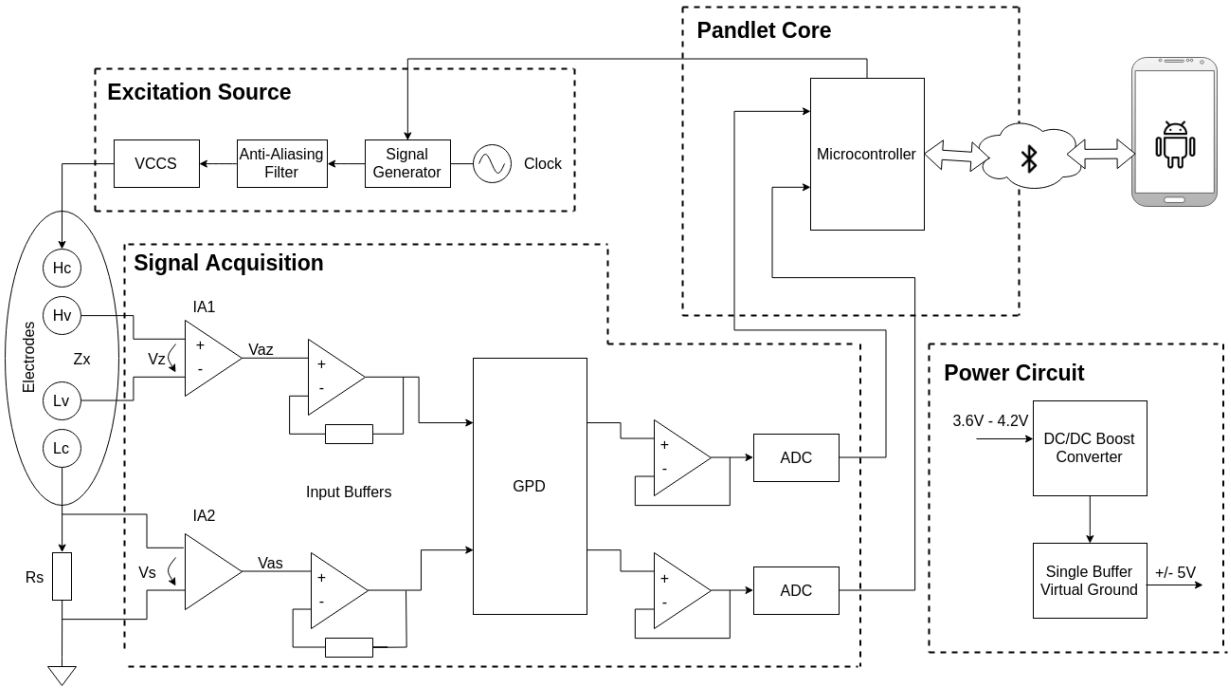

Figure 3.2: Structural diagram of the device.

3.2 Pandlet Core

Fraunhofer AICOS developed a novel architecture of embedded electronics for wireless devices platform named Pandlets, which stands for personal area networks letting everything sense. Pandlets are designed to be integrated with mobile platforms, as a basis for new Internet of Things (IoT) devices.

Taking modularity in mind the Pandlets hardware was designed to easily be adapted to different IoT need and applications. Pandlets is composed by several building block that when connected together create new devices and functionalities.

The Pandlet CORE (figure 3.3) is the basic building block and is the only used in this project. This Pandlet CORE is the heart of every Pandlet, because it is the one responsible for the radio, basic processing and sensing activities. The Pandlet CORE is composed by:

- ARM M0+, running at 16MHz
- Inertial Measurement Unit (IMU):

  - Accelerometer;
  - Gyroscope;
  - Magnetometer.

- Environmental Measurement Unit (EMU):
  - Humidity;
  - Pressure;
  - Temperature.

- Blueetooth Smart (fully compliant with Bluetooth Core Specification v4.0).

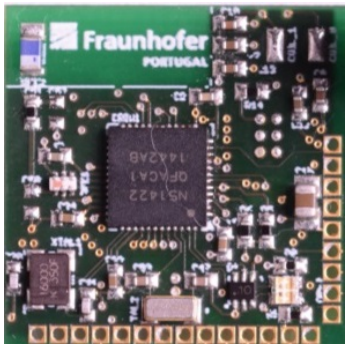

Figure 3.3: Pandlet Core.

The Pandlet CORE has a surface area of $28 \times 28mm$ and $1.0mm$ height, so it can be enclosed in a wide variety of off-the-shelf cases. Custom made enclosure designs, or textiles and clothes embedding is also a possibility.

The other building blocks that include Pandlet MEMORY and Pandlet SENSING+ are not object of study in this project since they are not used in the architecture of the device.

3.3 Excitation Source

3.3.1 Signal Generator

The signal generator is based on the Analog Devices AD9833, which is a low power, programmable waveform generator [12], that will be used for generating a multi frequency sine wave.

3.3.1.1 Theory of Operation

Sine waves are thought about in terms of their magnitude form: $a(t) = sin(\omega t)$. However they are nonlinear and not easy to generate except through piecewise construction. On the other hand the angular information is linear. The phase angle rotates through a fixed angle for each unit of time. The angular rate depends on the frequency of the signal in the following form: $\omega = 2\pi f$.

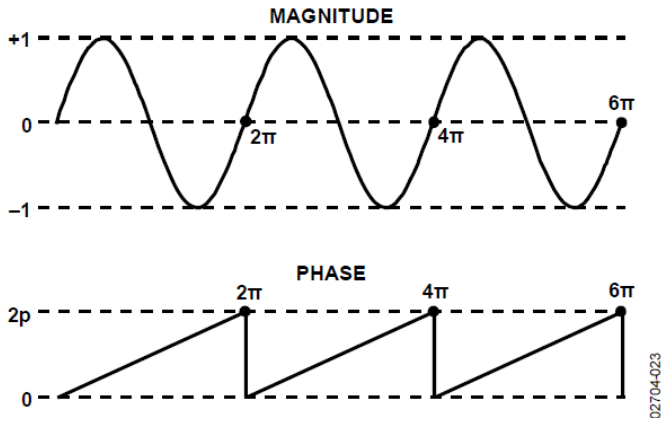

Figure 3.4: Typical Sine Wave. (In: [12])

Given a reference interval (clock period), the phase rotation for that period is:

$$\Delta Phase = \omega \Delta t \Leftrightarrow \omega = \Delta Phase/\Delta t = 2\pi f \Leftrightarrow f = \Delta Phase/\Delta t \times 2\pi \tag{3.1}$$

Substituting the reference clock frequency for the reference period $(1/f_{MCLK} = \Delta t)$.

$$f = \Delta Phase \times f_{MCLK}/(2\pi) \tag{3.2}$$

Based on this simple equation, the AD9833 chip builds the output.

3.3.1.2 Circuit Description

A simple fully integrated Direct Digital Synthesis (DDS) chip can implement equation (3.2), using three major subcircuits: Numerically Controlled Oscillator (NCO) and phase modulator, SIN ROM, and Digital-to-Analog Converter (DAC).

Numerically Controlled Oscillator Plus Phase Modulator

It is composed by two frequency select registers, a phase accumulator, two phase offset registers, and a phase offset adder. His main component is a 28-bit phase accumulator. Since time signals have a phase range between 0 and 2π, outside of this range, the sinusoid functions repeat themselves in a periodic manner. The accumulator simply scales the range of phase numbers into a multibit digital word, in the AD9833 the phase accumulator is implemented with 28 bits. Therefore $2\pi = 2^{28}$.

Substituting in equation (3.2):

$$f = \Delta Phase \times f_{MCLK}/2^{28} \tag{3.3}$$

where $0 < \Delta Phase < 2^{28} - 1$

The phase accumulator input can be selected either from the $FREQ0$ register or the $FREQ1$ register.

SIN ROM

The output from the NCO must be converted from phase information into sinusoidal value in order for it to be useful. Because phase information maps directly into amplitude, the SIN ROM uses the digital information as an address to a lookup table and converts the phase information into amplitude. From the 28 bits of the phase accumulator it only uses 12 truncated bits, because it is impractical having a lookup table of 2^{28} entries. It is only necessary to have sufficient phase resolution such that the errors due to truncation are smaller than the resolution of the 10-bit DAC.

Digital-to-Analog Converter (DAC)

The high impedance, current source 10-bit DAC receives the digital words from the SIN ROM and converts them into corresponding analog voltages. The output voltage range is typically $0.6V$ p-p.

The AD9833 also includes a voltage regulator because the digital section of the AD9833 is operated at $2.5V$ and the power supply can have a value of $2.3V$ to $5.5V$, this regulator steps down the power supplied.

3.3.1.3 Functionalities

AD9833 has a standard Serial Peripheral Interface (SPI) that allows the user to control and configure the chip by loading a 16-bit word through SPI.

When Powering up the AD9833 in order to avoid spurious DAC outputs the reset bit should be set to 1 and when the part is ready to begin operation this bit should be set to 1.

The chip contains a 16 bit control register that allows to configure the operation of the AD9833, in order to inform the AD9833 that the contents of the control register will be altered, bit 15 and 14 should be set to 0.

There are two frequency registers and two phase registers available and the analog output from the AD9833 is:

$$\frac{f_{MCLK}}{2^{28}} \cdot FREQREG \tag{3.4}$$

where $FREQREG$ is the value loaded in the frequency register and the signal is phase shifted:

$$\frac{2\pi}{4096} \cdot PHASEREG \tag{3.5}$$

where $PHASEREG$ is the value loaded in the phase register.

3.3.2 Anti-Aliasing Filter

The output from the signal generator contains useful sine wave signal but it also contains undesired alias signal [2]. Thus, an anti-aliasing filter is implemented using the LTC1560-1, which is a fully integrated continuous-time, lowpass filter [55].

The filter cutoff frequency, f_{CUTOFF}, is pin selectable to either $500kHz$ (Pin 5 to V+) or $1MHz$ (Pin 5 to V-). The LTC1560-1, unlike other high frequency filters, is designed for low noise and low distortion. In this application it is used a 5th order elliptic filter with a low pass cutoff frequency of $1MHz$.

3.3.3 Voltage Controlled Current Source

Multifrequency impedance measurement needs high-quality controlled current sources over a wide bandwidth ($10kHz - 1MHz$) even with large variations of the electrode contact impedances [56].

In this application the Current-Feedback Amplifier (CFA) AD844 is used, whose internal structure can be seen in figure 3.5 (shaded area), that has access to an internal high-impedance node (TZ) for external frequency compensation; this feature allows its use as a current conveyor.

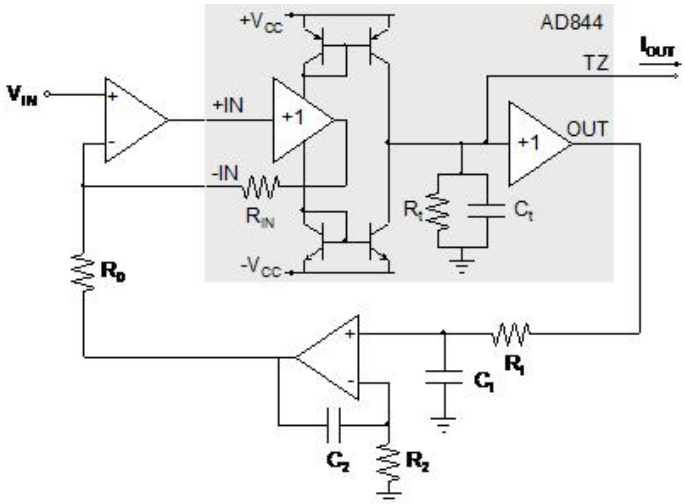

Figure 3.5: Voltage Controlled Current Source circuit. (In: [2])

The voltage applied to the high impedance non-inverting input is copied to the low-impedance inverting input, while the output is replicated by the mirrors and flows into the transimpedance $(Zt = Rt||Ct)$. The voltage developed across Z_t is buffered by the unity gain voltage follower. The transimpedance of the CFA (Zt) becomes the output impedance of the conveyor and the output of the VCCS.

If the AD844 were used only by itself, errors due to gain accuracy of the first stage and its non-zero output resistance R_{ob} are not overcome and another problem arises when applying any current source, the changing of the DC-blocking capacitor because of residual DC currents.

The circuit in figure 3.5 proposed by [56] overcomes these problems, by including an input buffer in the feedback loop of wideband op amp; in addition the output resistance of the resulting amplifier is virtually zero and adds no error to the intended transconductance. The DC output voltage before the capacitor is kept near $0V$ by using a DC feedback loop, which measures the actual DC voltage at the Z node and applies a correction to the input. This DC-feedback circuit must have a very high DC gain and a negligible gain at frequencies of interest. Their passive components are chosen in order to solve the trade-off between response time and low gain at the lower frequency to be injected to the load.

3.3.4 Reference Resistor

As can be observed in figure 3.6 a reference resistor (R_s) will be connected in series with Z_X (electrode connector), the voltage drop across this resistor will be later used as a reference by the GDP to calculate the magnitudes ratio and phase difference. Since 200Ω is the typical value of human tissues [57], a non-inductive resistor of this value was used as reference, connected to electrode L_C in the excitation loop.

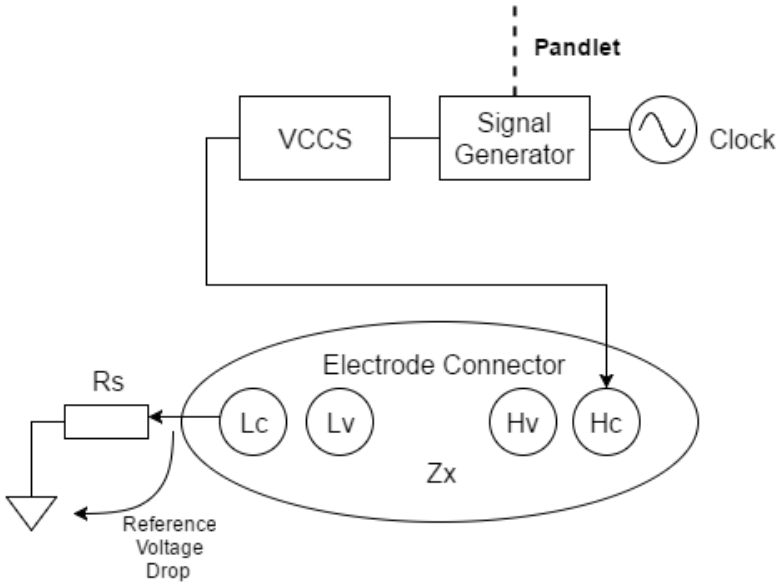

Figure 3.6: Excitation Loop. (In: [2])

3.4 Signal Acquisition

3.4.1 Instrumentation Amplifiers

A pair of instrumentation amplifiers are needed for measuring the voltage drop that will be sent to the GPD. As explained in section 3.3, a sinusoidal excitation current will flow through Z_X and R_s via a pair of current electrodes H_C and L_C. Another pair of voltage electrodes H_V and L_V will

detect the voltage drop across Z_X (V_X) and the instrumentation amplifier IA1 will amplify this value, while the voltage drop across Rs (Vs) is amplified by the second instrumentation amplifier IA2, as previously seen in figure 3.2.

The Texas Instruments INA163 was selected for both IA1 and IA2, which is a very low-noise, low-distortion, monolithic instrumentation amplifier with a high input impedance and wide frequency bandwidth [58].

The gain can be defined with the following equation:

$$G = 1 + \frac{6000}{R_G} \tag{3.6}$$

Using a gain resistor $R_G = 2k\Omega$ the gain was set to 4.

3.4.2 Input Buffers

Taking into account impedance matching between the amplified signal by the instrumentation amplifiers and the Gain Phase Detector which has an input impedance of 50Ω, two input buffers are needed. The decision was to use two high speed, low output impedance amplifiers Texas Instruments THS3061 [59] as unity gain buffer and a voltage attenuator with a 750Ω resistor and a 50Ω resistor (figure 3.7).

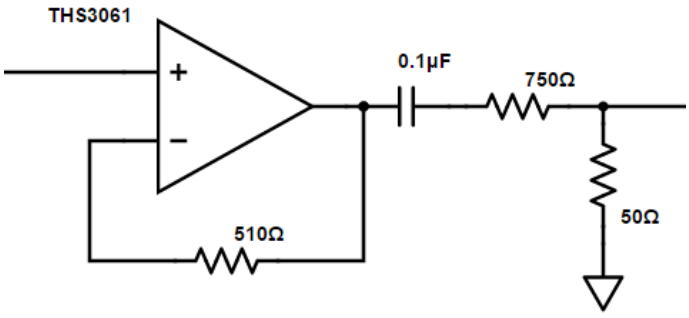

Figure 3.7: Input Buffers Circuit. (In: [2])

3.4.3 Gain Phase Detector

As the key component of the whole system for reliable measurement, GDP is based in the Analog Devices AD8302, which is a fully integrated system for measuring gain/loss and phase in numerous receive, transmit, and instrumentation applications. It provides an accurate measurement of either gain or loss over a $\pm 30dB$ range scaled to $30mV/dB$, and of phase over a $0° - 180°$ range scaled to $10mV/degree$ [13]. Its input range is -60 dBm ($316\mu V peak$) to 0 dBm ($316mV peak$) in a 50Ω system, having a large bandwidth (from low frequencies up to $2.7GHz$).

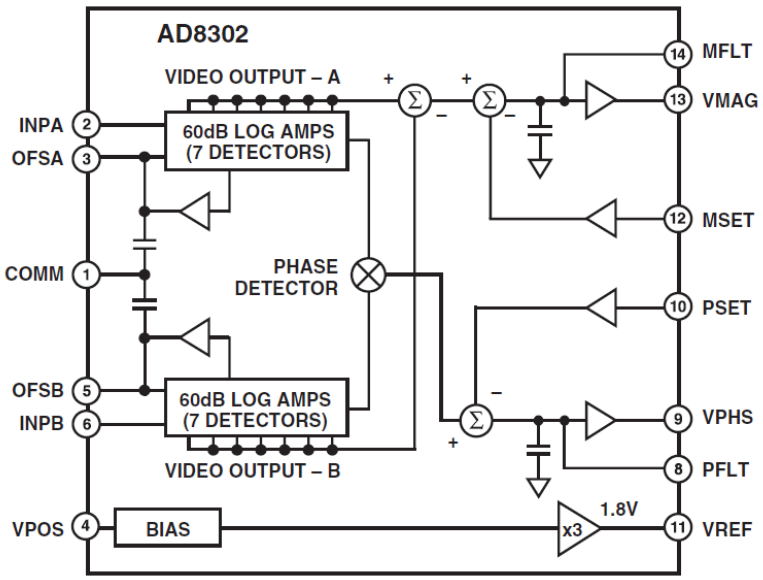

Figure 3.8: AD8302 Functional Block Diagram. (In: [13])

The AD8302 comprises a closely matched pair of demodulating logarithmic amplifiers, each having a 60 dB measurement range. By taking the difference of their outputs, a measurement of the magnitude ratio or gain between the two input signals is available.

The chip also includes a phase detector of the multiplier type, but with precise phase balance driven by the fully limited signals appearing at the outputs of the two logarithmic amplifiers making the phase accuracy measurement independent of signal level over a wide range.

A stable reference of $1.8V$ (output upper limit) is available at pin V_{REF} for precise repositioning of the output range.

3.4.3.1 Theory of Operation

Logarithmic amplifiers (log amps) provide a logarithmic compression function that converts a large range of input signal levels to a compact decibel-scaled output. The general mathematical form is:

$$V_{OUT} = V_{SLP} \cdot log\left(\frac{V_{IN}}{V_Z}\right) \tag{3.7}$$

where V_{IN} is the input voltage, V_Z is called the intercept (voltage), and V_{SLP} is called the slope (voltage). It is assumed throughout that $log(x)$ represents the $log_{10}(x)$ function. V_Z is the value of input signal that results in an output of zero and need not correspond to a physically realizable part of the log amp signal range.

The AD8302 takes the difference in the output of two identical log amps, each driven by signals of similar waveforms but at different levels. Since subtraction in the logarithmic domain corresponds to a ratio in the linear domain, the resulting output becomes:

$$V_{MAG} = V_{SLP} \cdot log\left(\frac{V_{INA}}{V_{INB}}\right) \tag{3.8}$$

where V_{INA} and V_{INB} are the input voltages, V_{MAG} is the output corresponding to the magnitude of the signal level difference, and V_{SLP} is the slope. Important to notice that V_Z has dropped out. Unlike the measurement of power, when measuring a dimensionless quantity such as relative signal level, no independent reference or intercept needs to be invoked.

The limited outputs from both log amps drive an exclusive-OR style digital phase detector. Operating strictly on the relative zero-crossings of the limited signals, the extracted phase difference is independent of the original input signal levels. The phase output has the general form:

$$V_{PHS} = V_\theta[\theta(V_{INA}) - \theta(V_{INB})] \tag{3.9}$$

where V_θ is the phase slope in $mV/degree$ and θ is each signal's relative phase in degrees.

3.4.3.2 Measurement Mode

Connecting the output pins, V_{MAG} and V_{PHS}, directly to the feedback setpoint input pins, M_{SET} and P_{SET}, the default slopes and center points are invoked; this connection is called measurement mode [13] (figure 3.9).

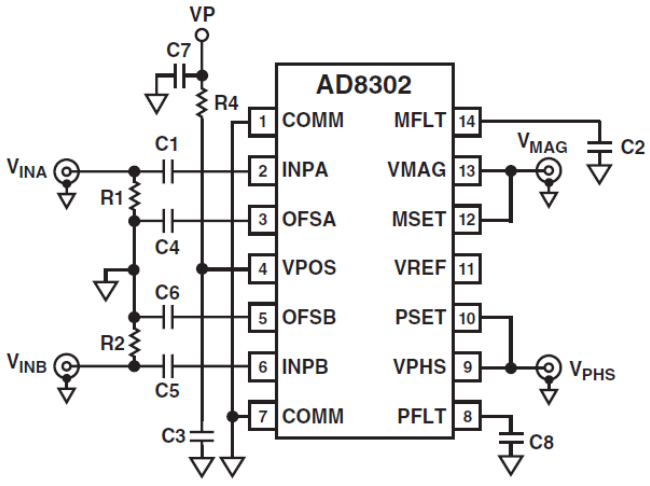

Figure 3.9: Connections in Measurement Mode. (In: [13])

A precise offset voltage of $900mV$ is introduced internally to establish the center-point (V_{CP}). In the low frequency limits in measurement mode, V_{MAG} and V_{PHS} can be expressed as:

$$V_{MAG} = R_F I_{SLP} \cdot log\left(\frac{V_{INA}}{V_{INB}}\right) + V_{CP} \tag{3.10a}$$

$$V_{PHS} = -R_F \cdot I_\theta(|\theta(V_{INA}) - \theta(V_{INB})| - 90^\circ) + V_{CP} \tag{3.10b}$$

where R_F is the transimpedance that represents the setpoint interface block. I_{SLP} and I_θ are characteristic slope current of the gain and phase detector, respectively.

For the gain function, the slope represented by $R_F I_{SLP}$ is $600mV/$decade or, dividing by $20dB/$decade, $30mV/$dB. With a center point of 900 mV for 0 dB gain, a range of -30 dB to $+30$ dB covers the full-scale swing from $0V$ to $1.8V$. For the phase function, the slope represented by $R_F I_\theta$ is 10 $mV/$degree. With a center point of 900 mV for 90°, a range of 0° to 180° covers the full-scale swing from $1.8V$ to $0V$. The range of 0° to $-180°$ covers the same full-scale swing but with the opposite slope.

Two $47\mu F$ capacitor were connected to the ac grounding pins OFSA and OFSB setting the corner frequency to $43Hz$ according to the formula $f_{HP}(MHz) = 2/C_C(nF)$, where C_C is the total capacitance from OFSA or OFSB to ground, including the internal $10pF$.

The magnitude ratio $|K|$ and phase differences θ in equations (3.11) can be solved from (3.10):

$$\begin{cases} |K| = \frac{|V_{AZ}|}{|V_{AS}|} = \frac{|V_{INA}|}{|V_{INB}|} = 10^{\frac{V_{MAG}-900mV}{600mV}} \\ \theta = (\theta_{V_{INA}} - \theta_{V_{INB}}) = \pm\left(\frac{900mV - V_{PHS}}{10mV/degree} + 90^\circ\right) \end{cases} \tag{3.11}$$

Taking into account that AD8302 does not distinguish between positive and negative phase differences and (3.10), the complex impedance formula (2.11) can be worked out in a polar-plane form:

$$\begin{cases} |Z_m| = R_S \cdot 10^{\frac{V_{MAG}-900mV}{600mV}} \\ \theta = -\left(\frac{900mV - V_{PHS}}{10mV/degree} + 90^\circ\right) \end{cases} \tag{3.12}$$

3.4.4 Analog-to-Digital Converter

MAX11612 is a low-power, 12-bit, multi channel ADC that can operate from a single supply of $4.5V$ to $5.5V$ [16]. The full-scale analog input range is determined by the internal reference ($4.096V$) or by an externally applied reference voltage ranging from $1V$ to V_{DD}. An external reference of $1.8V$ was chosen for use, supplied by the pin V_{REF} of the AD8302, defining the upper limit of the conversion.

This ADC features a Inter-Integrated Circuit (I2C) protocol consisting of a serial-data line (SDA) and a serial-clock line (SCL) that are connected to the Pandlets core.

Output buffers with unity gain are necessary between the outputs of AD8302 (V_{PHS} and V_{MAG}) feeding into the ADC, aiming to provide enough current driving for the ADC [2].

3.5 Power Circuit

The circuit configuration requires a $\pm 5V$ power supply. In order to achieve these differential values, a step-up conversion will need to be applied to the battery voltage ($V_{BAT} = 3.6 - 4.2V$) to $10V$ and by creating a virtual ground between $10V$ and the battery ground the required $\pm 5V$ are achieved.

The pandlet core is supplied with the $5V$ and reduced to $1.8V$ by an internal regulator. In order to communicate with the ADC (I2C) and the Signal Generator (SPI), two level shifters will be necessary to convert the $1.8V$ signals into $5V$ signals.

3.5.1 DC/DC Boost Converter

The TPS61040 is a high-frequency boost converter, capable of generating voltages up to $28V$ from a single-cell Li-Ion battery and has an internal $400mA$ switch current limit [14].

With a few external components (figure 3.10), we can define the output voltage, calculated by the following formula:

$$V_{OUT} = 1.233V \times \left(1 + \frac{R1}{R2}\right) \tag{3.13}$$

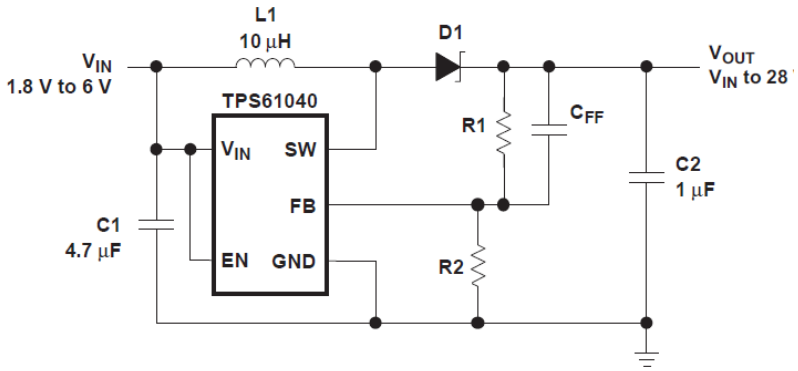

Figure 3.10: Typical Application Schematic (In: [14])

As stated before V_{OUT} was defined as $10V$, the feedforward capacitor and the inductor were calculated taking into account the peak current, maximum switching frequency and the rectifier diode forward voltage.

3.5.2 Single Buffer Virtual Ground

There is a requirement for a dual-voltage supply ($\pm 5V$) however there is only a single supply available.

One solution is based on the BUF634 that can drive up to $250mA$, that is a high speed, unity-gain open-loop buffer recommended for a wide range of applications [60].

As can be seen in figure 3.11, R_1 and R_2 create a "virtual ground", there are $10V$ across the circuit and the resistors are an $0.5\times$ resistive divider, having $5V$ at the midpoint of the divider. Between the midpoint of the divider and the negative side of the power supply there are $-5V$ and from the positive side of the power supply to the midpoint there there are $+5V$, providing two equal but opposite voltages from a single supply.

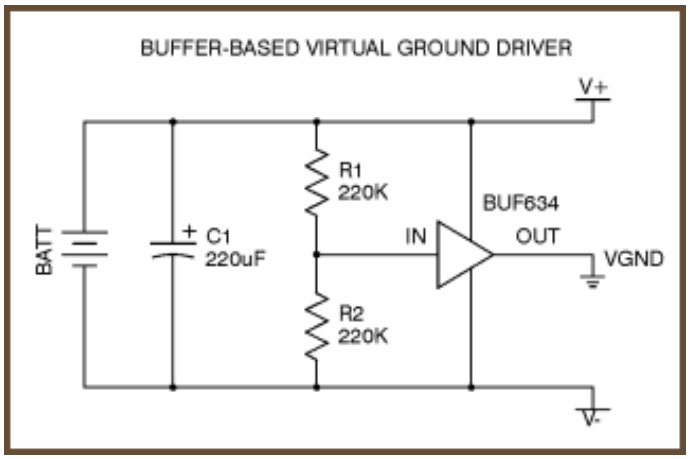

Figure 3.11: Buffer Virtual Ground Driver Circuit (In: [15])

Using BUF634 the virtual ground is buffered, making the voltage divider appear to have a very low impedance while still drawing little current, keeping the virtual ground centered between the positive and negative side.

3.5.3 I2C Level Shifter

The $1.8V$ signal on the Pandlet side needs to be translated into $5V$ to communicate with the ADC. TCA9406 is a 2-bit bidirectional I2C voltage-level translator with an output enable (OE) input [61].

On the A-side (Pandlet) the range of operation is from $1.65V$ to $3.6V$, referenced to V_{CCA}, and from $2.3V$ to $5.5V$ on the B-side (ADC), referenced to V_{CCB}.

The TCA9406 features internal $10k\Omega$ pullup resistors on SCL_A, SDA_A, SCL_B and SDA_B. In the application external pullup resistors were added to the B-side to reduce the total pullup resistance and speed up rising edges.

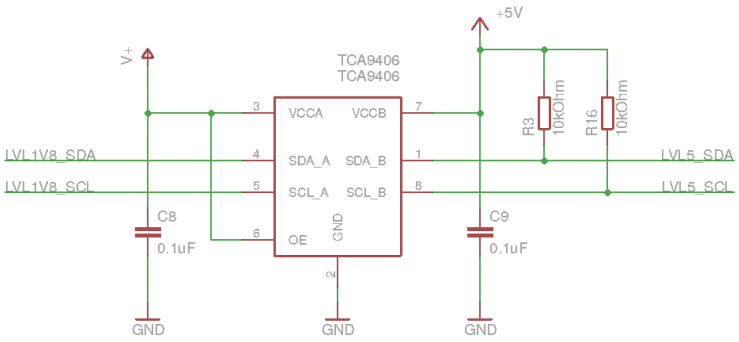

Figure 3.12: I2C Level Shifter schematic.

3.5.4 SPI level Shifter

The same problem as in the I2C arises in the SPI communication, since the signal from the Pandlet is at $1.8V$ and should be at $5V$. The TXB0104 device is a 4-bit, directionless voltage-level translator specifically designed for translating logic voltage levels [62].

The A port (Pandlet) accepts any supply voltage from $1.2V$ to $3.6V$. The B port accepts any supply voltage $1.65V$ to $5.5V$, allowing low-voltage bidirectional translation.

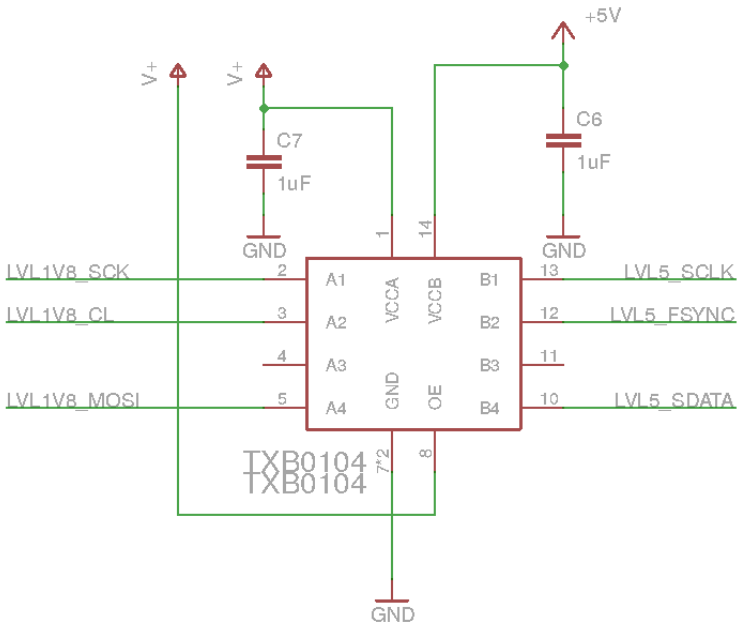

Figure 3.13: SPI Level Shifter schematic.

3.5.5 μUSB Charger

The design includes a Micro USB-B connector and a MCP73832 that is Li-Polymer Charge Management Controllers. The MCP73831/2 devices are highly advanced linear charge management controllers for use in space-limited, cost-sensitive applications [63].

In the last years portable electronics have played an important role, due to the characteristics of Li-Ion/Li-Polymer batteries, they are the most popular power sources for mobile devices. The system Power Path Management allows end-users to charge their batteries without interruption.

By including this μUSB charger in our device we allow the user to charge his battery autonomously just by connecting a μUSB cable to a power source.

Chapter 4

Implementation

4.1 Prototyping

The first stage of the implementation phase was to organize the different pieces in different groups, being the excitation source the one responsible for generating a current to be injected in the patient and the signal acquisition circuit responsible for measuring the voltage drop across the electrodes and calculating the phase and magnitude difference (figure 4.1).

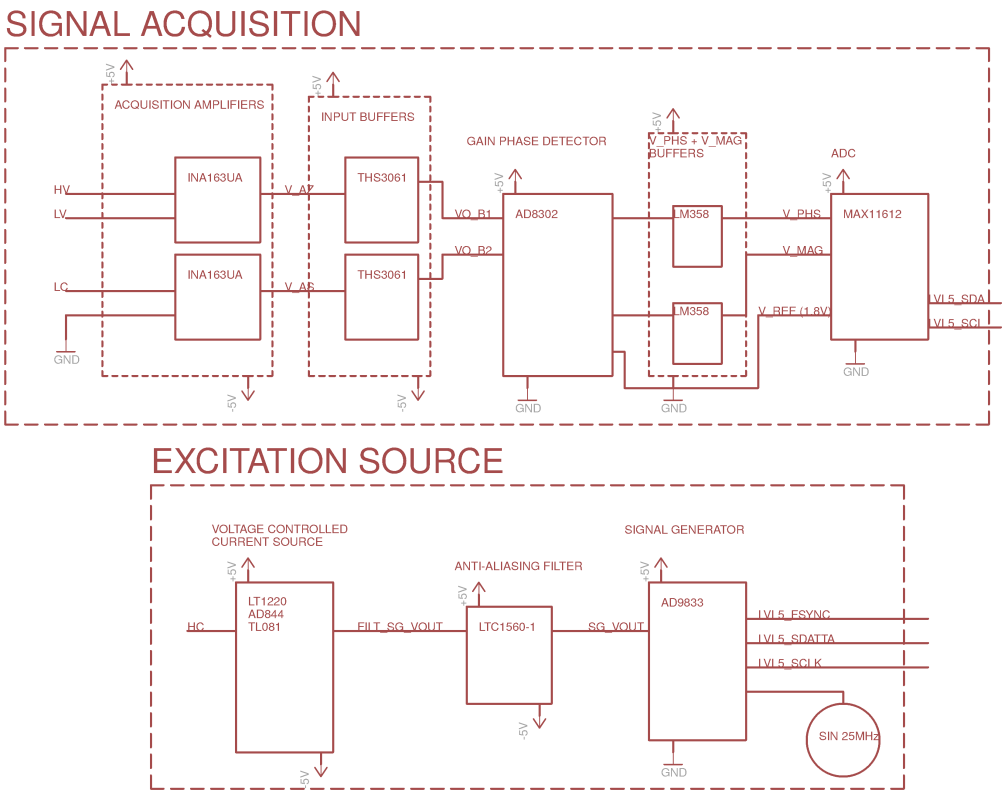

Figure 4.1: Circuit's two main groups.

A schematic was created, providing all the necessary details to build the electronics including how all the components are connected together. By specifying all the components it was possible to create the BoM for the development of the device.

An intermediate prototype was constructed using breadboards to connect the components of the excitation source and the signal acquisition circuit. For controlling the signal generator an Arduino UNO was used, due to its simplicity and flexibility. A DC Power Supply was used to provide energy to the prototype and an Oscilloscope allowed to validate independently the performance of each component.

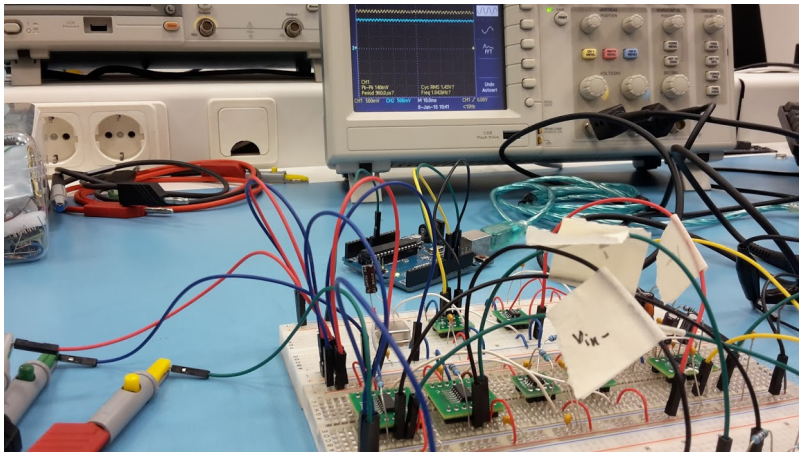

Figure 4.2: Intermediate prototype.

This prototype allowed the validation of the schematic and understanding how the different components worked, allowing the integration with the Pandlet Core. To make the device portable, a power circuit was later added to the design.

4.2 PCB Design

In medical devices it is important to assemble the circuit in a Printed Circuit Board (PCB) since usually the wiring introduces noise and errors to the measurement, thereafter reducing the diagnosis accuracy.

For the PCB design, the Eagle CAD software was used and as explained before. The PCB was designed around Pandlet Core; therefore a socket was placed in the PCB layout so the Pandlet Core could easily be connected to the PCB.

The layout is organized in three major sections: excitation source (center bottom), signal acquisition (top left corner) and power circuit (right side) (figure 4.3).

After reviewing the components' datasheets, all recommendations were followed and two different ground planes were created, one digital and one analog, the decoupling capacitors were placed close to the power pins. For the boost converter distinct planes were created as suggested in the datasheet (figure 4.4).

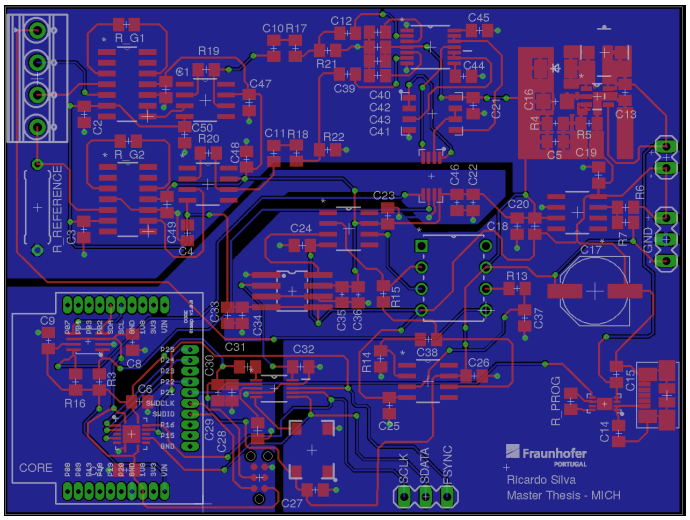

Figure 4.3: PCB layout.

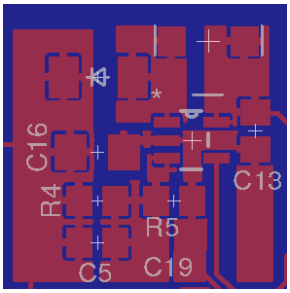

Figure 4.4: TPS61040 layout planes.

The power wires were designed with a width of 0.25*mm*, the signal lines with a width of 0.2*mm* and the vias with a drill of 0.3*mm*.

The Gerber files were then sent to a PCB producer and using a pick and place technique, the Surface Mount Devices (SMD) were assembled to the PCB.

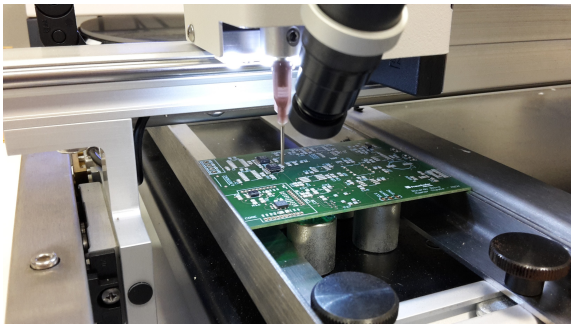

Figure 4.5: Assembly using pick and place technique.

4.3 I2C Protocol

The ADC (MAX11612) will communicate with the Pandlet Core via a I2C Protocol and it will only have two wires: SCL and SDA [16]. Since routines for writing and reading from the ADC were implemented, we provide next an explanation of how the ADC works and how the communication was handled.

I2C is a two-wire interface to connect low-speed devices like microcontrollers, EEPROMs, A/D and D/A converters, I/O interfaces and other similar peripherals in embedded systems. It was invented by Philips and now it is used by almost all major IC manufacturers and each I2C slave device needs an address that can be obtained from NXP (formerly Philips semiconductors) [64].

The master initiates a transmission with a START condition (S), a high-to-low transition on SDA while SCL is high. The master terminates a transmission with a STOP condition (P), a low-to-high transition on SDA while SCL is high (figure 4.6).

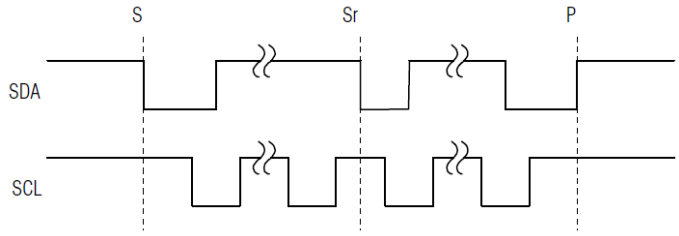

Figure 4.6: START and STOP Conditions. (In: [16])

Data transfers are acknowledged with an acknowledge bit (A) or a not-acknowledge bit (A). Both the master and the ADC (slave) generate acknowledge bits. To generate an acknowledge, the receiving device must pull SDA low before the rising edge of the acknowledge-related clock pulse (ninth pulse) and keep it low during the high period of the clock pulse (figure 4.7). To generate a not-acknowledge, the receiver allows SDA to be pulled high before the rising edge of the acknowledge-related clock pulse and leaves SDA high during the high period of the clock pulse.

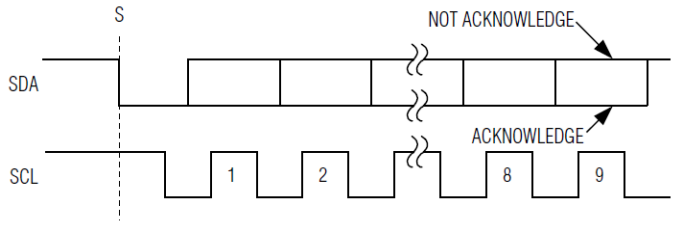

Figure 4.7: Acknowledge Bits. (In: [16])

Messages are broken up into two types of frames: an address frame, where the master indicatesto which slave the message is being sent, and one or more data frames, which are 8-bit data

messages passed from master to slave or vice versa. Data is placed on the SDA line after SCL goes low, and is sampled after the SCL line goes high.

A write cycle begins with the bus master issuing a START condition followed by seven address bits (figure 4.8), and a write bit (R/W = 0). If the address byte is successfully received, the ADC (slave) issues an acknowledge. The master then writes to the slave. The slave recognizes the received byte as the set-up byte, if the most significant bit (MSB) is 1. If the MSB is 0, the slave recognizes that byte as the configuration byte. The master can write either one or two bytes to the slave in any order. If the slave receives a byte successfully, it issues an acknowledge. The master ends the write cycle by issuing a STOP condition or a repeated START condition.

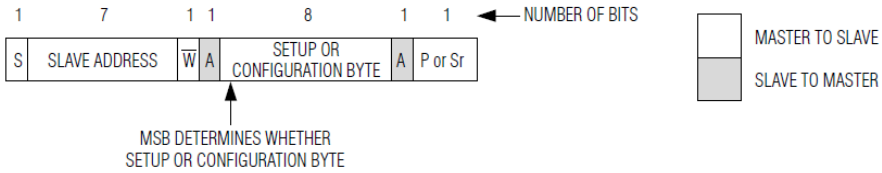

Figure 4.8: One Write Cycle. (In: [16])

A read cycle must be initiated to obtain the analog to digital conversion results. Read cycles begin with the bus master issuing a START condition followed by seven address bits and a read bit (R/W = 1). If the address byte is successfully received, the ADC (slave) issues an acknowledge. The master then reads from the slave. The result is transmitted in two bytes; first four bits of the first byte are high, then MSB through LSB are consecutively clocked out. After the master has received the byte(s), it can issue an acknowledge if it wants to continue reading or a not-acknowledge if it no longer wishes to read. If the ADC receive a not-acknowledge, they release SDA, allowing the master to generate a STOP or a repeated START condition.

4.4 SPI Protocol

As stated before, one of the critical parts of the system is the Signal Generator. This part is controlled by a SPI communication and in order to write to this chip, some SPI functions were implemented. In this section a presentation of the protocol and a explanation of how to interact with AD9833 will be made.

SPI is a synchronous protocol that allows a master device to initiate communication with a slave device. Data is exchanged between these devices [65].

In SPI, since it is a Synchronous protocol, the data is clocked along with a clock signal (SCK) that controls when data is changed and when it should be read. The clock signal is provided by the master to provide synchronization. The clock signal controls when data can change and when it is valid for reading.

Often a slave select signal will control when a device is accessed. This signal is known as the SS signal and stands for “Slave Select.” It indicates to a slave that the master wishes to start an SPI

data exchange between that slave device and itself. The signal is most often active low, so a low on this line will indicate the SPI is active, while a high will signal inactivity.

When data is sent from the master to a slave, it is sent on a data line called MOSI, for “Master Out / Slave In”. If the slave needs to send a response back to the master, the master will continue to generate a prearranged number of clock cycles, and the slave will put the data onto a third data line called MISO, for “Master In / Slave Out”.

As seen in subsection 3.3.1, AD9833 is controlled through a standard SPI communication. As such, only 3 wires will be needed, since there’s no need for a MISO data line because AD9833, that works as a slave, do not need to send data, only receive [12].

Data is loaded into the device as a 16-bit word under the control of a serial clock input, SCK.

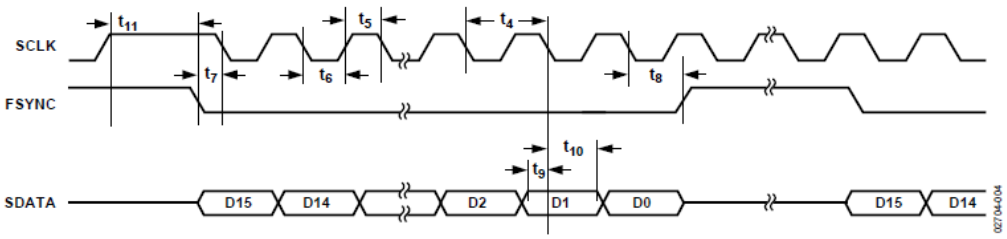

Figure 4.9: Serial Timing. (In: [12])

The SS input, from now on called FSYNC, is a level triggered input that acts as a frame synchronization and chip enable. Data can be transferred into the device only when FSYNC is low. To start the serial data transfer, FSYNC should be taken low. After that, data is shifted into the input shift register of the device on the falling edges of SCK for 16 clock pulses. FSYNC may be taken high after the 16th falling edge of SCK.

SCK can be continuous, or it can idle high or low between write operations. In either case, it must be high when FSYNC goes low.

4.5 Bluetooth Low Energy

In section 2.8 we analysed some Low Power Technologies and concluded that BLE can be implemented without losing the low-power and portability that are the main goals of this work. In this section will be described how a custom service was defined so the different BLE functionalities could be implemented; this service is presented in the attribute table 4.1:

Table 4.1: Implemented Attribute Table

	Handle	**UUID Type of Attribute**	**Attribute Permission**	**Atrribute Value**
Service Declaration	0x000X	Service Declaration Standard UUID 0x2800	Read Only, No Authentication, No Authorization	Custom Service UUID
Characteristic Declaration	0x000X	Characteristic Declaration Standard UUID 0x2803	Read Only, No Authentication, No Authorization	Properties: Notify Value Handle (0x000X), Custom Characteristic UUID
Characteristic Value Declaration	0x000X	UUID found in the Characteristic Declaration Value	Read Only, No Authentication, No Authorization	Phase and Gain Value
Descriptor Declaration	0x000X	Client Characteristic Configuration Descriptor (CCCD) Standard UUID 0x2902	Read and Write, No Authentication, No Authorization	Notification Enabled 0x00-XX
Characteristic Declaration	0x000X	Characteristic Declaration Standard UUID 0x2803	Read Only, No Authentication, No Authorization	Properties: Write Value Handle (0x000X), Custom Characteristic UUID
Characteristic Value Declaration	0x000X	UUID found in the Characteristic Declaration Value	Write Only, No Authentication, No Authorization	Start/Cancel Measurement Command

At the top of every attribute table one finds the Service Declaration attribute. Its type is always 0x2800 which is the standard UUID for Service Declarations. Its permissions are always Read Only without any authentication or authorization required. The value is our custom service UUID.

The Characteristic Declaration is similar to the Service Declaration. The type is always 0x2803, the standard UUID for Characteristic Declarations. And the permissions are always Read Only without any authentication or authorization required. The Value contains a handle, a UUID, and a set of properties describe the subsequent Characteristic Value Declaration. The handle points to the Characteristic Value Declaration's place in the attribute table. The UUID descibes what type of information or value can be expected to find in the Characteristic Value Delcaration and the properties describe how the characteristic value can be interacted with.

The Characterisitic Value Declaration is the attribute that contains the actual value and in the attribute table implemented (table 4.1) it is defined an attribute with notify properties that will be used to send to the Android App the Phase and Magnitude values measured by the device and another attribute with write properties that will allow to send to the Pandlet an instruction to start the measurement.

The Descriptor Declaration is an attribute with additional information about the characteristic. In this situation it is used the Client Characteristic Configuration Descriptor (CCCD) that is writable descriptor that allows the client to enable or disable notification or indication.

The Handle of each attribute will be dependent of how many attributes are already present in the table.

4.6 Firmware

The firmware framework implements a set of basic functions that must be performed by the base module processor, like functions for sensors and peripherals communication, access to communication bus, implementation of efficient energy management mechanisms and also Bluetooth radio communications protocol implementation.

In this context, the nRF51 Software Development Kit (SDK) was considered, provided by Nordic Semiconductor. This SDK contains all the drivers, libraries, examples and Application Programming Interfaces (APIs) needed. Among the libraries used, these can be highlighted:

- Debug Logger – enables debug logs;
- Schedule Handling – used for transferring execution from the interrupt context to the main context;
- Timer – enables the application to create multiple timer instances;
- Communications libraries – adds I2C and SPI functions to the Pandlet.

The nRF51 SDK also has a precompiled linked binary software, which implements the Bluetooth Low Energy stack, called SoftDevice (SD). The proprietary profiles were implemented using

this SD and new features can be added to Pandlets using Over-the-Air (OTA) updates using the bootloader provided.

Nordic implemented other SDs that provide Central Role that can be used to allow the Pandlets to connect with other devices using Bluetooth Low Energy.

To provide access to the API, Nordic uses an ARM feature called Supervisor Call (SVC) to access functions inside the binary of the SD. Those functions range from BLE interactions (discovery, characteristics management, pairing/bonding, etc.) using the Protocol Stack, SD management (enabling/disabling SD, Scheduler, Events, etc.) using the SoftDevice Manager and SoC features access (Interrupts management, peripherals, etc.) using SoC Library. Most of these features are encapsulated in ready to use libraries that ease their integration to the developer's app.

All of this is developed over the nRF51 HW, and the application was built by integrating everything together.

4.6.1 State Machine

The most important tasks of our device are asynchronous and some of them are event-driven, creating a State Machine is an efficient way to guarantee a robust code, figure 4.10.

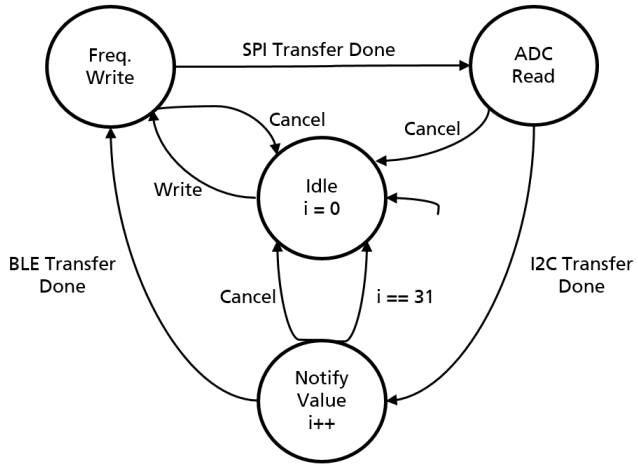

Figure 4.10: State Machine.

Initially the device is in an Idle State, when the Write instruction is sent by the user by SPI the frequency is written to the Signal Generator, initializing the measurement. Only when the SPI transfer is done, the value can be read from the ADC by I2C, this ensures that we are reading the Phase and Magnitude of the correct frequency. When the I2C transfer is finished we can notify through BLE the measured values. When the BLE transfer ends we go back to the Frequency Write State, this cycle is done 32 times, each one for a different frequency, after completing the measurement it goes back to Idle State, and is ready to start another measurement.

At any time the user can cancel the measurement by sending a Cancel instruction, going back to the Idle State.

4.7 Android App

Android 4.3 (API Level 18) introduces a built-in platform support for Bluetooth Low Energy in the central role and provides APIs that apps can use to discover devices, query for services, and read/write characteristics [66].

4.7.1 Main Features

In this section we will discuss the main features that were introduced with Android 4.3 by describing the classes and methods that allow us to perform Bluetooth communications.

The BluetoothAdapter class is required for any and all Bluetooth activity. The Bluetooth Adapter represents the device's own Bluetooth adapter (the Bluetooth radio), it allows to perform fundamental Bluetooth tasks, such as initiate device discovery and query a list of bonded (paired) devices.

To find BLE devices, it is used the $startLeScan()$ method. This method takes a $LeScanCallback$ as a parameter. This callback needs to be implemented, because that is how scan results are returned. Some guidelines need to be followed since power consumption is the key and scanning is battery-intensive: after finding the device it is important to stop scanning; never scan on a loop and create a time limit for scanning.

To start interacting with a BLE device the first step is connecting to it, more specifically, connecting to the GATT server on the device. Using the $connectGatt()$ method we can connect to the GATT server hosted by the BLE device returning a BluetoothGatt instance that can later be used to conduct GATT client operations.

With the Android BLE API it is possible to interact with the BLE device, and a group of classes and methods allows for example to connect, read and write BLE attributes and receive GATT notifications.

4.7.2 Integration

Based on the Android Developer Bluetooth LE sample [67] an Android App was developed with the functionalities to instruct the device to start the measurement and to display the data measured by the device.

The first step to start a BLE connection is to scan for devices using the $startLeScan()$ method previously described, an activity for scanning for BLE devices was created allowing only to display devices selected by the developer, in this situation our device.

After selecting the device a connection will be created between the measuring device and the smartphone. The next activity allows to start and cancel the measurement by writing to the device. When the "Start Measurement" is pressed a value of $0xAA$ is written in the Characteristic Value Declaration Attribute, if the "Cancel Measurement" button is pressed a value of $0xFF$ is written to the same attribute. This values are then received by the measurement device that start or cancel the measurement according to the value received.

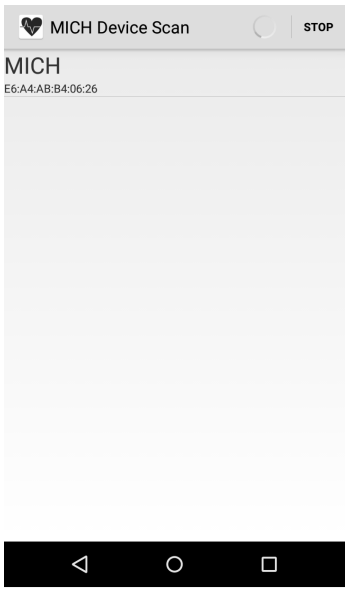

Figure 4.11: Scan Activity.

When the measurement is finished another activity pops up allowing the user to select if he wants to see the Phase or Magnitude graph. The hexadecimal values transmitted from the measurement device are then converted to voltage using the ADC transfer function and using equation (3.12) the actual Phase and Magnitude values are calculated.

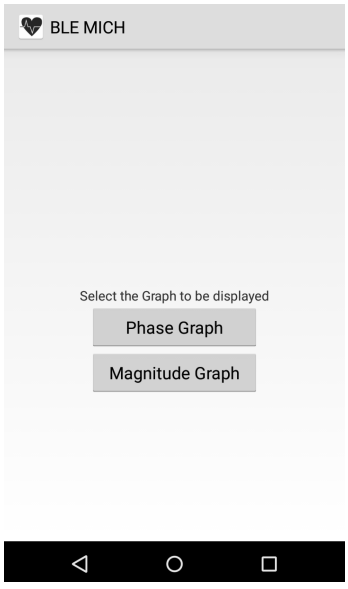

Figure 4.13: Graph Select Activity.

Using the Androidplot library two different graphs were displayed providing the measurement values already converted to Phase (degree) and Magnitude (Ω) over the frequencies of the measurement (kHz).

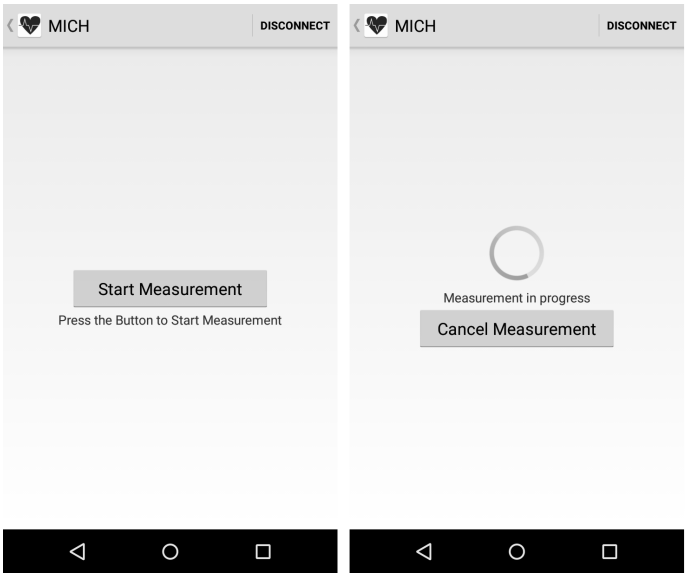

Figure 4.12: Start and Cancel Activity.

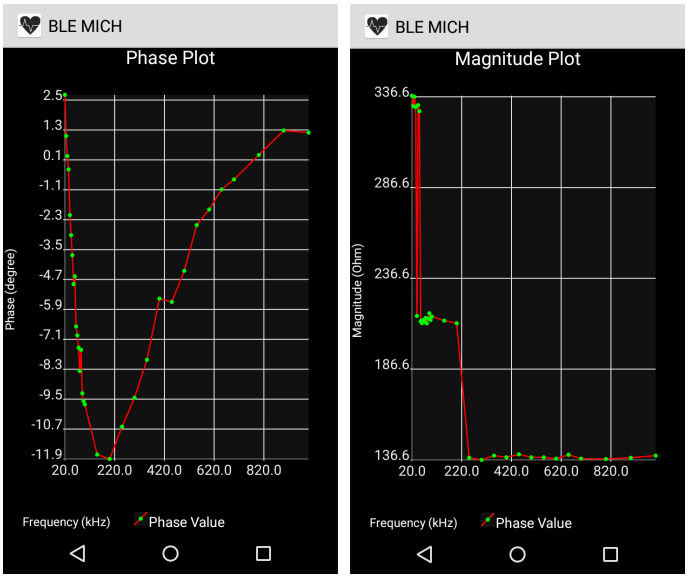

Figure 4.14: Phase and Magnitude Graph Display Activity.

Chapter 5

Results

This chapter will evaluate the performance of the measurement device by performing some measurements using a RC circuit, with the hypothesis that the ECF and ICF act like resistors and the cell membrane like an capacitor in biological tissues, as seen in section 2.1. The goal of this measurement is to evaluate the robustness of the measuring device in a controlled environment.

An evaluation of the platform will be carried by discussing the advantages of the measuring device when compared with the solutions available in the market.

5.1 Measurement Analysis

In order to evaluate the performance of the system, five different RC circuits were prepared (figure 5.1); the nominal values of R_1, R_2 and C are described in table 5.1, and the cutoff frequency is given by equation (5.1) as proposed by [2].

$$fc = \frac{1}{2\pi C} \cdot \sqrt{\frac{R_1 + R_2}{R_1 R_2^2}} \tag{5.1}$$

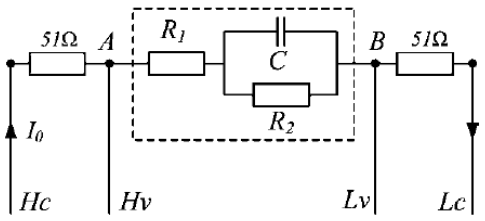

Figure 5.1: Four-terminal topology of the RC circuit measurements. (In: [2])

In these circuits the two 51Ω resistors are used to simulate the resistance between the current output and voltage measurement electrodes.

Table 5.1: Parameters of the five measurements.

Measurement Number	$R_1(\Omega)$	$R_2(\Omega)$	$C(nF)$	$fc(kHz)$
1	150	150	10	150
2	200	200	10	113
3	200	200	68	16.6
4	300	300	68	11
5	270	270	10	83

Each circuit was measured within a range of 32 frequencies from $20kHz$ to $1MHz$ logarithmically spaced (20, 25, 30, 35, 40, 45, 50, 55, 60, 65, 70, 75, 80, 85, 90, 95, 100, 150, 200, 250, 300, 350, 400, 450, 500, 550, 600, 650, 700, 800, 900, 1000 kHz). It is important to space the frequencies logarithmically to ensure a proper density of data [68]. The values of Phase and Magnitude were stored in a CSV file and the phase-frequency (figure 5.2) and magnitude-frequency (figure 5.3) characteristics were plotted.

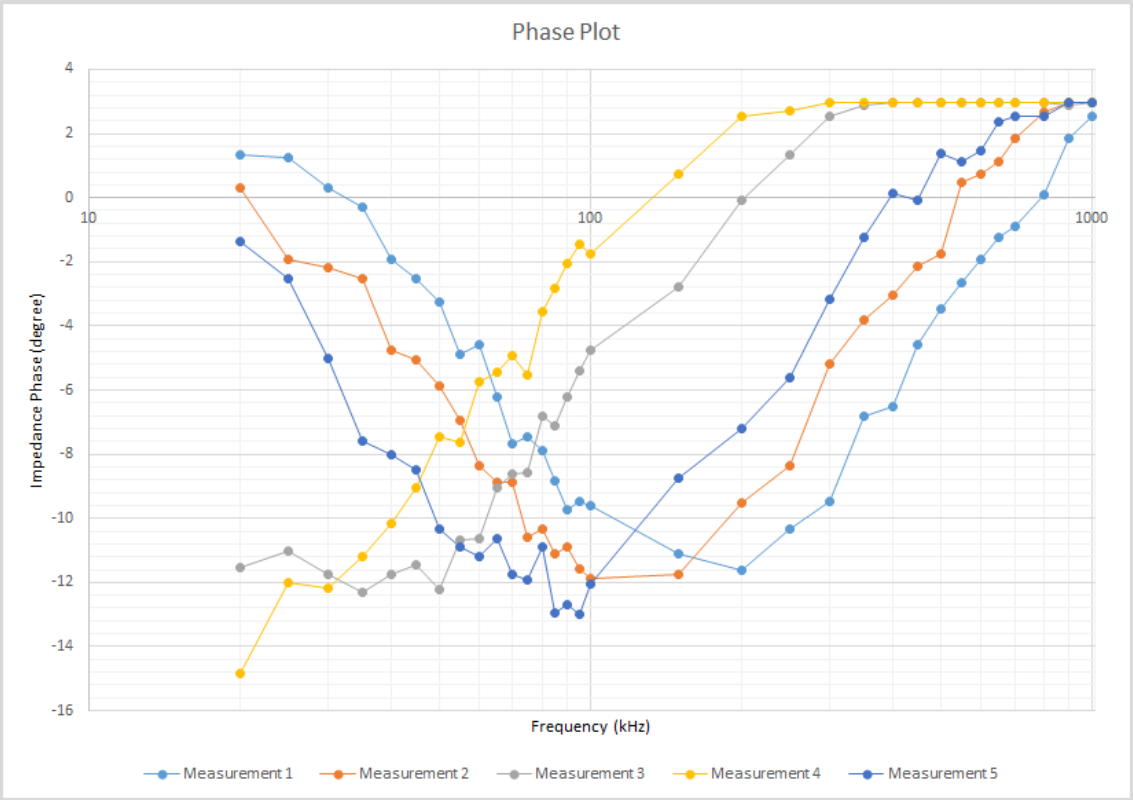

Figure 5.2: Impedance Phase Plot.

we

It is possible to observe in the phase plot that the characteristic frequency is the point where the phase has its minimal value. This can be observed in the measurements 1, 2 and 5 as the cutoff frequency increases the plot moves proportionally. In the measurements 3 and 4 the cutoff frequency is below the $20kHz$, this was previously reported by Yuxiang Yang et al. [2]. Due to electronic

constraints our device cannot perform measurements below $20kHz$ whereas bioimpedance spectra below $20kHz$ contains useful information [69].

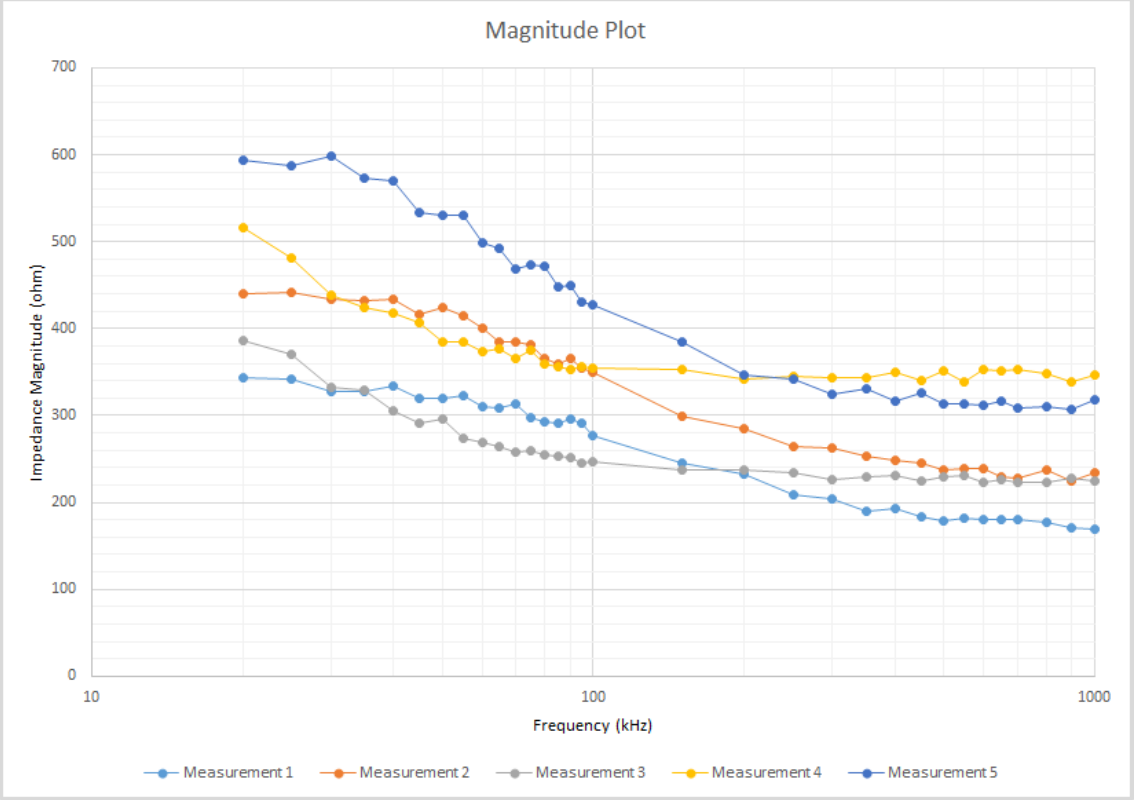

Figure 5.3: Impedance Magnitude Plot.

In the first stage (low frequencies) the capacitor in the RC circuit works as an open circuit and after the cutoff frequency it starts to work as a short circuit. This can be verified in the magnitude plot, for example in measurement 1 below the cutoff frequency ($150kHz$) the magnitude is approximately 330Ω (the sum of both resistors) while after $150kHz$, it decreases to approximately 170Ω (only R_1).

When comparing the values of the different RC circuits with the values of the measurements it is easy to identify similarities. However measurement errors are nearly inevitable, random errors in measurements can be eliminated by performing a set of measurements and calculate the average, but systematic errors could only be eliminated for example by calibration.

5.2 Averaging Review

As noticed in section 5.1, some random errors reduce the accuracy of our prototype, and these errors can be introduced for example by the ADC conversion errors.

By making more measurements for each frequency and averaging these values, a more accurate result will be obtained and the curves will be smoother. The difficulty to find the number of

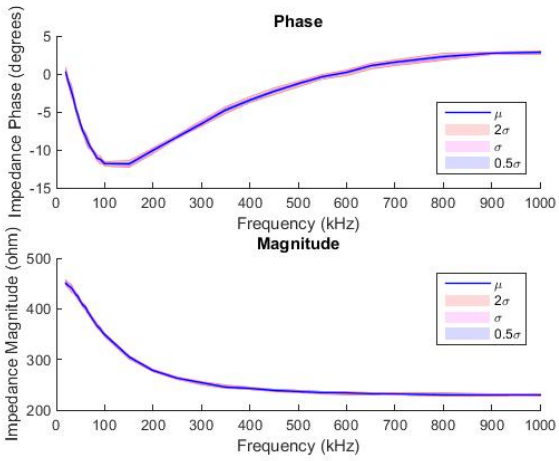

(a) 10 Samples Group.

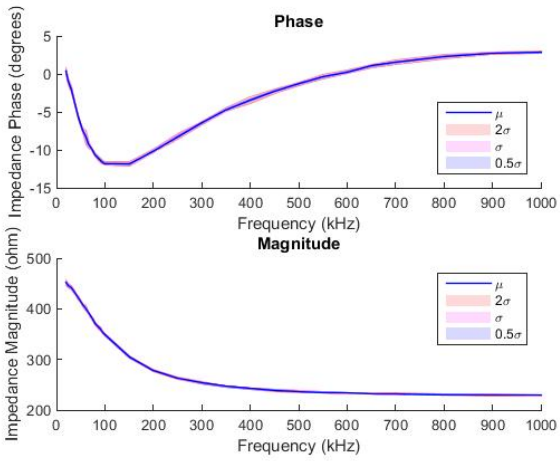

(b) 20 Samples Group.

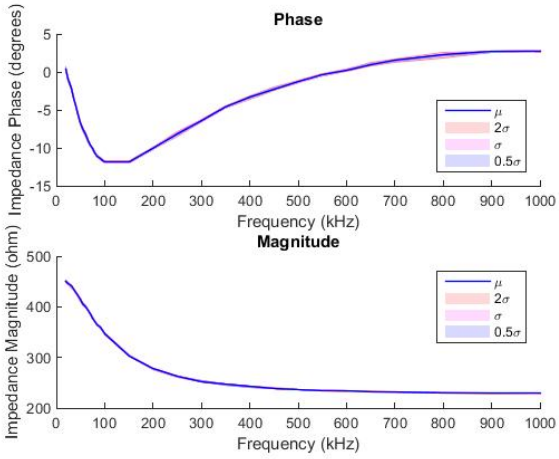

(c) 50 Samples Group.

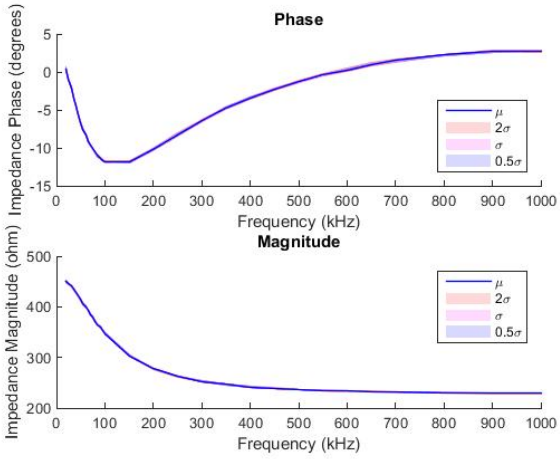

(d) 100 Samples Group.

measurements needed to have a good result motivated us to perform an averaging test. Four each of the 32 frequencies we acquire 10, 20, 50, and 100 samples. Then for each frequency the average value was calculated. This test was repeated 40 times for each number of samples (i.e. 10, 20, 50, and 100) and the values were stored in a CSV file.

Using the MATLAB function shadedErrorBar [70] the average of the 40 measurements for each number of samples was calculated and plotted, this function also creates a continuous shaded error region around the mean value.

By observing the plots of the averaging test it is possible to notice that by averaging 10 samples the result is satisfactory, since the shaded area is really small, and as we increase the number of samples the curve becomes smoother.

The number of collected samples will increase the time of the measurement, consequently spending more battery, but this result in more accurate measurement. We leave the decision of the number of samples to be collected to the user, that will need to consider the trade-off between measurement quality and battery lifetime.

5.3 Platform Evaluation

At the time the project began to be developed the main goals were to develop a low-cost and portable solution with an easy to use interface that could be operated by a big range of users. Regarding the portability, two aspects were taken in consideration: the size and the power consumption.

During the development it was decided to develop a PCB with the size of $80 \times 60mm$ (figure 5.5). Most of the chips used were SMD so it could be saved some space.

The system has a power consumption of $260mA$ when in idle state and it goes to $280mA$ during measurements. The battery used is a Lithium-ion Polymer rechargeable battery, considering a power consumption of approximately $270mA$ (alternating between idle and measurement state). Each measurement takes only 1.4 seconds, during a battery life approximately 220 measurements can be done [71].

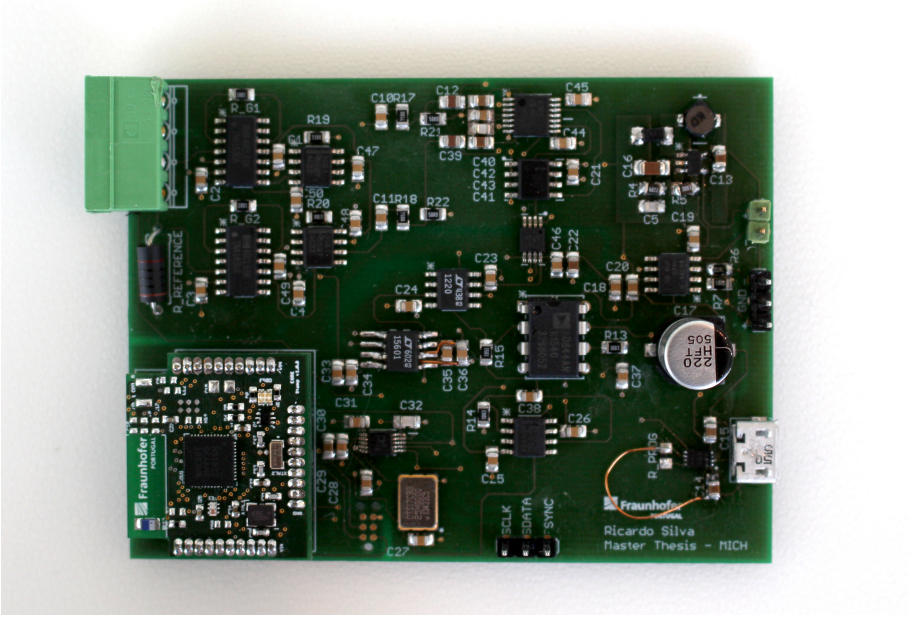

Figure 5.5: Measurement Device Assembled.

The BoM of the measuring device is of 147,11$ and the price of its PCB is 102,91$; this price could be decreased in a next version by developing a minor version using passive components of smaller sizes.

The Pandlets Core developed by Fraunhofer has a production price of 22$, but the fact that this measuring device can be integrated in a bigger solution of multiparameter monitoring, being the Pandlet Core the “heart” of this system makes its price insignificant.

Our end-to-end solution is completed with the Android App allowing the user to start the measurement and previously receive the values of the measurement. By linking this device with a smartphone the additional cost of inserting a display in the device can be cut out and no additional

knowledge to understand the device operation is needed, since nowadays most of the population have a smartphone and knows how to operate it.

Chapter 6

Conclusions and Future Work

This thesis aimed to develop a method for measuring the bioelectrical impedance of the thorax so fluid overload in the lungs could be detected long before hospitalization due to Heart Failure.

By using multifrequency measurement method like Bioelectrical Impedance Spectroscopy a lot more information was provided about the tissue properties which helped to get better results in the measurement.

The MRPDD technique allowed to simplify the electronics providing a wide frequency range, small circuitry dimensions, small power consumption; being this a cost effective alternative to the classical methods.

The power circuit created was responsible to supply the Pandlets Core and the measurement device, it allowed the system to be supplied by a Lithium-ion Polymer rechargeable battery, not needing to be connected to a plug.

The use of a BLE communication proved to be very efficient due to its low-cost and low-power consumption, adding the fact that was possible to use the Pandlet for this communication, a hybrid solution was created, once that in the future this measuring device can be integrated in a multi parameter monitoring system.

An user friendly Android App provides an easy way for the patient to monitor his status without needing to operate a medical device and the values of the measurement can be later saved in a database or sent to the caregiver or the medical clinician.

The results obtained in the test measurements allowed to conclude the validity of the system, tested in different conditions in a controlled environment. The next step will be to test in a clinical environment with the supervision of a medical specialist.

There are some solutions available in the market, but the fact that they are expensive and have a big size makes them not suitable for a user to have them at home or continuously monitor himself. During the development of this project two aspects were always kept in mind: the portability and the low-cost solution. Both of these goals were achieved, having in the end a small size and low power device for less than 300$ that can be carried anywhere.

6.1 Future Work

Although almost all goals were achieved, there is always something more to be done and some aspects to improve, such as:

- System Calibration - After removing the random errors it is important to make sure the systematic errors introduced mainly from the analog input/outputs channels. This can be achieved by calibrating the entire system;
- Cole Parameters Extraction - By applying some nonlinear models to the complex impedance it is possible to extract these parameters, as seen in section 2.3, however this approach requires more processing power;
- Body Fluid Volumes Estimation - After finding the Cole Parameters it is possible to estimate the body fluid volume of an individual, this is the parameter of most interest to physicians;
- Reduce the device size - The actual size is already satisfactory, however after testing the first PCB, if a next version is developed this size can be decreased by reducing the size of passive components and arrange the components in an improved layout;
- Improvements in the Android App - User login, database to store the measurements values and a tutorial for how to apply the electrodes are examples of some features that could be introduced in a next version;
- Clinical Setting Tests - A daily monitoring of heart failure patients will allow a final validation of the device.

References

[1] Lisa Beckmann, Dirk van Riesen, and Steffen Leonhardt. Optimal electrode placement and frequency range selection for the detection of lung water using bioimpedance spectroscopy. In *Engineering in Medicine and Biology Society, 2007. EMBS 2007. 29th Annual International Conference of the IEEE*, pages 2685–2688. IEEE, 2007.

[2] Yuxiang Yang, Jue Wang, Gang Yu, Feilong Niu, and Ping He. Design and preliminary evaluation of a portable device for the measurement of bioimpedance spectroscopy. *Physiological Measurement*, 27(12):1293, 2006.

[3] David Ayllon, Fernando Seoane, and Roberto Gil-Pita. Cole equation and parameter estimation from electrical bioimpedance spectroscopy measurements-a comparative study. In *2009 Annual International Conference of the IEEE Engineering in Medicine and Biology Society*, pages 3779–3782. IEEE, 2009.

[4] Tushar Kanti Bera. Bioelectrical impedance methods for noninvasive health monitoring: A review. *Journal of Medical Engineering*, 2014.

[5] Kazunari Okada and Toshimasa Sekino. Impedance measurement handbook. *Agilent Technologies*, 128:5950–3000, 2003.

[6] S Talha Ahsan and H McCann. Digital phase-sensitive detector (psd) as accumulator-sampler and its implementation in fpga. *Sci. Int.(Lahore)*, 26(1):65–73, 2014.

[7] Medical Dewata Website. http://medicaldewata.com/product.php?id_product=48. [Online; accessed 5-January-2016].

[8] *XiTRON Hydra 4200 Brochure*. XiTRON Technologies 9770-A Carroll Centre Road San Diego, CA 92126 USA.

[9] Physio Flow Website. http://www.physioflow.com/. [Online; accessed 3-January-2016].

[10] NUMED Website. http://www.numed.me/products/detail/?page=1356. [Online; accessed 5-January-2016].

[11] *ZOE Monitor User Manual*. 6412 S. Arville Street Las Vegas, NV 89118.

[12] Analog Device. Ad9833 datasheet, 2003.

[13] AnaLog Devices. Ad8302 datasheet, 2001.

[14] Texas Instruments. Tps61040 datasheet, 2015.

[15] Virtual Ground Circuits - TangentSoft Website. https://tangentsoft.net/elec/vgrounds.html. [Online; accessed 2-June-2016].

[16] Maxim Integrated. Max11612 datasheet, 2012.

[17] Tamara B. Horwich Anh L. Bui and Gregg C. Fonarow. Epidemiology and risk profile of heart failure. *Nat Rev Cardiol*, 8(1):30–41, jan 2011.

[18] Teresa Mota Humberto Morais Fernando Matias António de Sousa Fátima Ceia, Cândida Fonseca and António Gouveia Oliveira. Prevalence of chronic heart failure in southwestern europe: the epica study. *The European Journal of Heart Failure 4*, pages 531–539, 2002.

[19] Andreas P. Kalogeropoulos Catherine Norton, Vasiliki V. Georgiopoulou and Javed Butler. Epidemiology and cost of advanced heart failure. *Progress in Cardiovascular Diseases*, 54(2):78–85, 2002.

[20] Lyn Folan and Marjorie Funk. Measurement of thoracic fluid content in heart failure. *AACN Advanced Critical Care*, 19(1):47–55, 2008.

[21] MD W. H. Wilson Tang and MSc Wilson Tong. Measuring impedance in congestive heart failure: Current options and clinical applications. *Am Heart J*, 157(3):402–411, mar 2009.

[22] Meyler S Kazatzker M Mosseri M Frimerman A Rabinovich P Shotan A Shochat M, Charach G and Meisel S. Internal thoracic impedance monitoring: a novel method for the preclinical detection of acute heart failure. *Cardiovasc Revasc Med*, 7(1):41–45, 2006.

[23] Wang L and Patterson R. Multiple sources of the impedance cardiogram based on 3-d finite difference human thorax models. *IEEE Trans Biomed Eng*, 42(2):141–148, 1995.

[24] Frank H. Netter. *Atlas of Human Anatomy*. Book Distributors Inc, second edition, 1997.

[25] James J. Ackmann. Complex bioelectric impedance measurement system for the frequency range from 5 hz to 1 mhz. *Annals of Biomedical Engineering*, 21:135–146, 1993.

[26] T. ; Caffarel J. ; Kelkboom E. ; Aarts R. ; Korsten E. ; Cleland J Torabi, A. ; Mabote. Sensitivity of a wearable bioimpedance monitor to changes in the thoracic fluid content of heart failure patients. *Computing in Cardiology Conference*, pages 927–930, sep 2013.

[27] Kenneth S. Cole. Permeability and impermeability of cell membranes for ions. *Cold Spring Harb Symp Quant Biol*, 8:110–122, 1940.

[28] Mark Ulbrich, Jens Muhlsteff, Daniel Teichmann, Steffen Leonhardt, and Marian Walter. A thorax simulator for complex dynamic bioimpedance measurements with textile electrodes. *Biomedical Circuits and Systems, IEEE Transactions on*, 9(3):412–420, 2015.

[29] Orjan G Martinsen and Sverre Grimnes. *Bioimpedance and bioelectricity basics*. Academic press, 2011.

[30] Stefan Dantchev and Feras Al-Hatib. Nonlinear curve fitting for bioelectrical impedance data analysis: a minimum ellipsoid volume method. *Physiological measurement*, 20(1):N1, 1999.

[31] Yuxiang Yang, Wenwen Ni, Qiang Sun, He Wen, and Zhaosheng Teng. Improved cole parameter extraction based on the least absolute deviation method. *Physiological measurement*, 34(10):1239, 2013.

[32] Michel Y Jaffrin and Hélène Morel. Body fluid volumes measurements by impedance: A review of bioimpedance spectroscopy (bis) and bioimpedance analysis (bia) methods. *Medical engineering & physics*, 30(10):1257–1269, 2008.

[33] T. K. Bera and J. Nagaraju. Electrical impedance spectroscopic study of broiler chicken tissues suitable for the development of practical phantoms in multifrequency eit. *Journal of Electrical Bioimpedance*, 2:48–63, 2011.

[34] C. K. Meador E. C. Hoffer and D. C. Simpson. Correlation of whole-body impedance with total body water volume. *Journal of Applied Physiology*, 27(4):531–534, 1969.

[35] W.W. Bolonchuk H. C. Lukaski, P. E. Johnson and G. I.Lykken. Assessment of fat-free mass using bioelectrical impedance measurements of the human body. *American Journal of Clinical Nutrition*, 41(4):810–817, 1985.

[36] ESR Gopal et al. Principles of emulsion formation, 1968.

[37] Jan Nyboer, Marian M Kreider, and Leonard Hannapel. Electrical impedance plethysmography a physical and physiologic approach to peripheral vascular study. *Circulation*, 2(6):811–821, 1950.

[38] D. K. Swanson and J. G. Webster. Origin of the electrical impedance pulse in the limbs. *Proceedings of the 29th Annual Conference on Engineering in Medicine & Biology*, 18:324, 1976.

[39] John E Strobeck, Marc Silver, and Hector Ventura. Impedance cardiography: noninvasive measurement of cardiac stroke volume and thoracic fluid content. *Congestive Heart Failure*, 6(2):56–59, 2000.

[40] Marcos HF Ribeiro, Rodrigo Weber dos Santos, Luis Paulo S Barra, and Franciane C Peters. Simulation study on the determination of cardiac ejection fraction by electrical impedance tomography using a hybrid heuristic approach. *Journal of Medical Imaging and Health Informatics*, 4(1):113–121, 2014.

[41] Tushar Kanti Bera and Nagaraju Jampana. A multifrequency constant current source suitable for electrical impedance tomography (eit). In *Systems in Medicine and Biology (ICSMB), 2010 International Conference on*, pages 278–283. IEEE, 2010.

[42] *BioZ Operator's Manual*. 6175 Nancy Ridge Drive San Diego, California 92121 USA.

[43] *HYDRA ECF/ICF (Model 4200) Operation Manual*. 9770-A Carrol Centre, San Diego, CA 92121, USA.

[44] *Quantum-IV Features and Specifications*. 33939 Harper Avenue Clinton Township MI 48035 USA.

[45] William T Abraham, Steven Compton, Garrie Haas, Blair Foreman, Robert C Canby, Robert Fishel, Scott McRae, Gloria B Toledo, Shantanu Sarkar, and Douglas A Hettrick. Intrathoracic impedance vs daily weight monitoring for predicting worsening heart failure events: results of the fluid accumulation status trial (fast). *Congestive Heart Failure*, 17(2):51–55, 2011.

[46] Sarwat I Chaudhry, Yongfei Wang, John Concato, Thomas M Gill, and Harlan M Krumholz. Patterns of weight change preceding hospitalization for heart failure. *Circulation*, 116(14):1549–1554, 2007.

[47] LifeWave Biomedical Website. http://www.lifewavebiomed.com/Technology. [Online; accessed 3-January-2016].

[48] Comparing Low-Power Wireless Technologies - DigiKey Website. http://www.digikey.pt/en/articles/techzone/2011/aug/comparing-low-power-wireless-technologies. [Online; accessed 7-June-2016].

[49] Connectivity Options Explained - Activity Tracker World Website. http://activitytrackerworld.com/connectivity-options-explained/. [Online; accessed 7-June-2016].

[50] The Fundamentals Of Short-Range Wireless Technology - Electronic Design Website. http://electronicdesign.com/communications/fundamentals-short-range-wireless-technology. [Online; accessed 7-June-2016].

[51] What is Zigbee RF4CE? - RF Wireless World Website. http://www.rfwireless-world.com/Terminology/what-is-zigbee-RF4CE.html. [Online; accessed 7-June-2016].

[52] Geoff Mulligan. The 6lowpan architecture. In *Proceedings of the 4th workshop on Embedded networked sensors*, pages 78–82. ACM, 2007.

[53] Jonas Olsson. 6lowpan demystified. *Texas Instruments*, 2014.

[54] Kevin Townsend, Carles Cufí, Robert Davidson, et al. *Getting started with Bluetooth low energy: tools and techniques for low-power networking*. " O'Reilly Media, Inc.", 2014.

[55] Linear Technology. Ltc1560-1 datasheet, 1997.

[56] Ramon Bragos, Javier Rosell, and Pere Riu. A wide-band ac-coupled current source for electrical impedance tomography. *Physiological measurement*, 15(2A):A91, 1994.

[57] Henry C Lukaski and William A Siders. Validity and accuracy of regional bioelectrical impedance devices to determine whole-body fatness. *Nutrition*, 19(10):851–857, 2003.

[58] Texas Instruments. Ina163 datasheet, 2000.

[59] Texas Instruments. Ths3061 datasheet, 2009.

[60] Texas Instruments. Buf634 datasheet, 2015.

[61] Texas Instruments. Tca9406 datasheet, 2014.

[62] Texas Instruments. Txb0104 datasheet, 2014.

[63] Microchip. Mcp7383x datasheet, 2014.

[64] I2C Info – I2C Bus, Interface and Protocol. http://i2c.info/. [Online; accessed 3-June-2016].

[65] Overview and Use of the PICmicro Serial Peripheral Interface - Microchip Website. http://ww1.microchip.com/downloads/en/devicedoc/spi.pdf. [Online; accessed 3-June-2016].

[66] Android Developers - Bluetooth Low Energy. https://developer.android.com/guide/topics/connectivity/bluetooth-le.html. [Online; accessed 10-June-2016].

[67] Android Developers - Bluetooth Low Energy Sample. https://developer.android.com/samples/BluetoothLeGatt/index.html. [Online; accessed 10-June-2016].

[68] Andreoli De Lorenzo, A Andreoli, J Matthie, and P Withers. Predicting body cell mass with bioimpedance by using theoretical methods: a technological review. *Journal of Applied Physiology*, 82(5):1542–1558, 1997.

[69] Markus Osypka and Eberhard Gersing. Tissue impedance spectra and the appropriate frequencies for eit. *Physiological measurement*, 16(3A):A49, 1995.

[70] MathWorks Website - shadedErrorBar. https://www.mathworks.com/matlabcentral/fileexchange/26311-shadederrorbar. [Online; accessed 10-July-2016].

[71] Battery Life Calculator - Digikey Website. http://www.digikey.pt/en/resources/conversion-calculators/conversion-calculator-battery-life. [Online; accessed 25-June-2016].